THE PAndAS VIEW OF THE ANDROMEDA SATELLITE SYSTEM. II. DETAILED PROPERTIES OF 23 M31 DWARF SPHEROIDAL GALAXIES

Nicolas F. Martin[1,2], Rodrigo A. Ibata[1], Geraint F. Lewis[3], Alan McConnachie[4], Arif Babul[5], Nicholas F. Bate[6], Edouard Bernard[7], Scott C. Chapman[8], Michelle M. L. Collins[9], Anthony R. Conn[3], Denija Crnojević[10], Mark A. Fardal[11], Annette M. N. Ferguson[12], Michael Irwin[6], A. Dougal Mackey[13], Brendan McMonigal[3], Julio F. Navarro[5], and R. Michael Rich[14]

[1] Observatoire astronomique de Strasbourg, Université de Strasbourg, CNRS, UMR 7550, 11 rue de l'Université, F-67000 Strasbourg, France; nicolas.martin@astro.unistra.fr
[2] Max-Planck-Institut für Astronomie, Königstuhl 17, D-69117 Heidelberg, Germany
[3] Sydney Institute for Astronomy, School of Physics A28, The University of Sydney, NSW 2006, Australia
[4] NRC Herzberg Institute of Astrophysics, 5071 West Saanich Road, Victoria, BC V9E 2E7, Canada
[5] Department of Physics and Astronomy, University of Victoria, Victoria, BC V8P 1A1, Canada
[6] Institute of Astronomy, University of Cambridge, Madingley Road, Cambridge CB3 0HA, UK
[7] Laboratoire Lagrange UMR 7293, Université de Nice Sophia-Antipolis, CNRS, Observatoire de la Côte d'Azur, CS 34229, F-06304, Nice Cedex 04, France
[8] Department of Physics and Atmospheric Science, Dalhousie University, Coburg Road, Halifax, NS B3H 1A6, Canada
[9] Department of Physics, University of Surrey, Guildford, Surrey GU2 7XH, UK
[10] Physics Department, Texas Tech University, Lubbock, TX 79409, USA
[11] Department of Astronomy, University of Massachusetts, Amherst, MA 01003, USA
[12] Institute for Astronomy, University of Edinburgh, Blackford Hill, Edinburgh EH9 3HJ, UK
[13] Research School of Astronomy and Astrophysics, Australian National University, Canberra, ACT 2611, Australia
[14] Department of Physics and Astronomy, University of California, Los Angeles, PAB, 430 Portola Plaza, Los Angeles, CA 90095-1547, USA

ABSTRACT

We present a comprehensive analysis of the structural properties and luminosities of the 23 dwarf spheroidal galaxies that fall within the footprint of the Pan-Andromeda Archaeological Survey (PAndAS). These dwarf galaxies represent the large majority of Andromeda's known satellite dwarf galaxies and cover a wide range in luminosity ($-11.6 \lesssim M_V \lesssim -5.8$ or $10^{4.2} \lesssim L \lesssim 10^{6.5} L_\odot$) and surface brightness ($25.1 \lesssim \mu_0 \lesssim 29.3$ mag arcsec^{-2}). We confirm most previous measurements, but we find And XIX to be significantly larger than before ($r_h = 3065^{+1065}_{-935}$ pc, $M_V = -10.1^{+0.8}_{-0.4}$) and cannot derive parameters for And XXVII as it is likely not a bound stellar system. We also significantly revise downward the luminosities of And XV and And XVI, which are now $M_V \sim -7.5$ or $L \sim 10^5 L_\odot$. Finally, we provide the first detailed analysis of Cas II/And XXX, a fairly faint system ($M_V = -8.0^{+0.4}_{-0.3}$) of typical size ($r_h = 270 \pm 50$ pc), located in close proximity to the two bright elliptical dwarf galaxies NGC 147 and NGC 185. Combined with the set of homogeneous distances published in an earlier contribution, our analysis dutifully tracks all relevant sources of uncertainty in the determination of the properties of the dwarf galaxies from the PAndAS photometric catalog. We further publish the posterior probability distribution functions of all the parameters we fit for in the form of MCMC chains available online; these inputs should be used in any analysis that aims to remain truthful to the data and properly account for covariance between parameters.

Key words: galaxies: dwarf – Local Group

Supporting material: tar.gz file

1. INTRODUCTION

The stellar content of dwarf galaxies, their dynamical, kinematic, and chemical properties, and their spatial distribution around and their rate of infall onto their host can all be linked to the faint end of galaxy formation in a cosmological model (e.g., Mateo 1998; Grebel & Gallagher 2004; Gilmore et al. 2007; Sales et al. 2007; Tolstoy et al. 2009; McConnachie 2012; Weisz et al. 2014b; Pawlowski & McGaugh 2014). However, for a long time, the small number of dwarf galaxies known to inhabit the Local Group, where these dim systems can be studied with the most detail, limited the extent of insight they could provide.

At the turn of the century, panoramic photometric CCD surveys opened up the realm of low surface brightness stellar structures. Not only did these surveys provide the means to discover much dimmer dwarf galaxies (see, e.g., McConnachie 2012; Belokurov 2013 for reviews; see Willman & Strader 2012 for some of the questions these new systems raise), but the homogeneity of these surveys provided the means to build samples of dwarf galaxy properties free of the systematics that usually stem from observing different stellar systems with different instruments and studying them with different analytic techniques. The reader is referred to, e.g., Martin et al. (2007), Simon & Geha (2007), de Jong et al. (2008), or Weisz et al. (2014a) for both spectroscopic and photometric studies that strive to take such global approaches to infer the properties of Milky Way dwarf galaxies and, therefore, limit the impact of systematics. One such example that is particularly relevant to this paper is the work of Martin et al. (2008, hereafter M08), who presented a comprehensive study of the structural and luminosity-related properties of all the Milky Way dwarf galaxies found in the Sloan Digital Sky Survey (SDSS) at the time. This study further proposed to eschew binning and smoothing and rely instead on the information carried by every star present in the photometric catalog of a dwarf galaxy through the expression of the likelihood of families of structural models.

Around the Andromeda galaxy (M31), new dwarf galaxies were revealed by successive photometric surveys with increasing coverage. Such surveys include a dedicated SDSS stripe along the major axis of M31 (e.g., Zucker et al. 2004) and a survey of the inner halo of the galaxy with the INT/WFC (Ferguson et al. 2002; Irwin et al. 2008). These efforts culminated in a systematic, deep surveying of the region within 150 kpc of M31 for the Pan-Andromeda Archaeological Survey (PAndAS; McConnachie et al. 2009; Ibata et al. 2014) that led to the discovery of 16 new dwarf galaxies (Martin et al. 2006, 2009, 2013a; Ibata et al. 2007; McConnachie et al. 2008; Richardson et al. 2011). Beyond the PAndAS footprint, additional surveys continue to reveal new systems (Bell et al. 2011; Slater et al. 2011; Martin et al. 2013b, 2013c), yet without reaching the depth achieved by PAndAS. In total, 24 proposed dwarf spheroidal galaxies ($-12 \lesssim M_V \lesssim -6$) lie within the PAndAS footprint. As such, the homogeneous view of the M31 surroundings provided by this survey brings forth a unique opportunity to build a homogeneous set of properties for a large majority of the known dwarf galaxy satellites of the Andromeda galaxy. Conn et al. (2011, 2012a) have initiated this endeavor by determining tip-of-the-red-giant-branch (TRGB) distances for all the Andromeda satellites in the PAndAS footprint. We now extend this effort to provide a complete list of structural parameters and luminosity-related properties for all these dwarf galaxies.

The paper is structured as follows: Section 2 presents the PAndAS data used for the analysis of the dwarf galaxies, Section 3 explains our statistical framework to infer the properties of the dwarf galaxies, and Section 4 describes our results and compares them with those of past studies. The paper is summarized in Section 5.

This contribution is the second in a series of PAndAS papers focusing on dwarf galaxies in the PAndAS footprint. Paper I focused on an automated search for M31's dwarf galaxies in the PAndAS data (Martin et al. 2013a), while Paper III derives the dwarf galaxy search completeness limits within the PAndAS footprint (N. F. Martin et al. 2016, in preparation).

2. DATA

The specifics of the design, acquisition, reduction, and calibration of the PAndAS survey have been explained in detail in previous contributions from our collaboration (e.g., Ibata et al. 2014), and we shall not revisit these here. It is, however, worth mentioning that this Canada–France–Hawaii Telescope (CFHT) Large Program was built on two previous CFHT surveys led by R. Ibata and A. McConnachie (Ibata et al. 2007; McConnachie et al. 2008), which were further complemented by ~230 hr of observation with the same wide-field imager, MegaCam, in order to cover a contiguous region of ~390 deg² within ~150 kpc of M31 and ~50 kpc of its companion M33. Each one of the 1 deg² MegaCam fields was observed for at least 45 minutes in both the MegaCam g and i bands, under exquisite conditions (median seeing of 0″.67 and 0″.60, respectively, for the two bands). The final (5σ) depths of the survey are 26.0 and 24.7, respectively, with some variations from field to field (Ibata et al. 2014). In the analysis, we only use the catalog of aperture magnitudes, and these are dereddened following Equation (1) of Ibata et al. (2014) when needed. We also always use the stellarity flags to keep only star-like objects, as defined in the same publication.

The dwarf galaxy sample we focus on here comprises all the dwarf spheroidal galaxies that fall in the PAndAS footprint, as
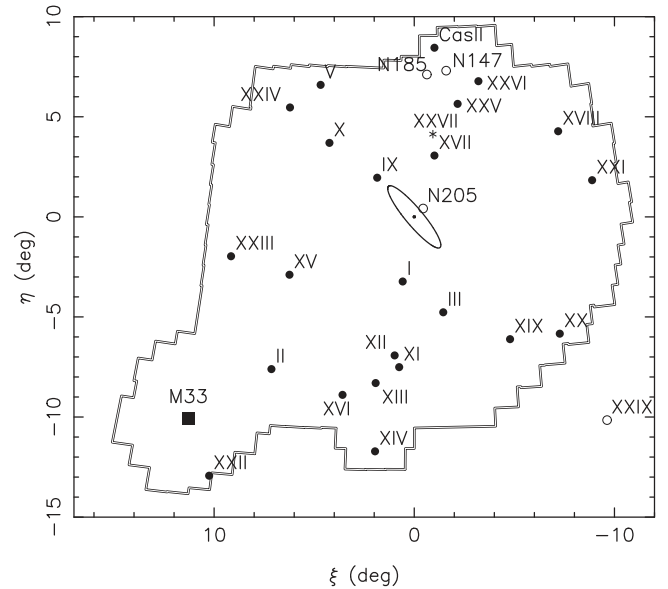

Figure 1. Distribution of dwarf galaxies around M31, whose disk is represented by the central ellipse. North is to the top and east to the left. M33 is represented by the large square in the bottom left corner. The polygon represents the PAndAS footprint, and all dwarf galaxies studied in this paper are shown as filled circles, except for the peculiar And XXVII, located by the asterisk. Other dwarf galaxies are shown as open circles.

seen in Figure 1: And I, And II, And III, And V, And IX, And X, And XI, And XII, And XIII, And XIV, And XV, And XVI, And XVII, And XVIII, And XIX, And XX, And XXI, And XXII, And XXIII, And XXIV, And XXV, And XXVI, and the latest PAndAS discovery Cas II/And XXX. The brightest dwarf galaxy satellites of M31 (M32, NGC 205, NGC 147, and NGC 185) are beyond the scope of this paper as their complexity, the crowding they suffer from, and/or their location in the survey render their study difficult and require dedicated analyses. The reader is referred to Crnojević et al. (2014) for a detailed study of NGC 147 and NGC 185. The case of And XXVII, which was originally included in the current analysis, is discussed in detail in Section 4.24, as our results lead us to the conclusion that it is likely not a bound dwarf galaxy.

Figure 2 presents the color–magnitude diagrams (CMDs) of all the dwarf galaxies in the sample. All the CMDs include stars within two elliptical half-light radii of a galaxy's centroid[15] as inferred through our algorithm described below. The great variety of M31 dwarf galaxies is readily visible in this figure, with the brightest systems at the top corresponding to discoveries made from photographic plate studies (And I, And II, And III, And V; van den Bergh 1972; Armandroff et al. 1998), followed by systems discovered as overdensities of red giant branch (RGB) stars with CCD surveys and photometry: And IX and And X in the SDSS (Zucker et al. 2004, 2007), And XIV in a series of isolated M31 outer halo fields (Majewski et al. 2007), And XVII in the INT/WFC survey that preceded PAndAS (Irwin et al. 2008), and all the other ones from pre-PAndAS or PAndAS photometry (Martin et al. 2006, 2009; Ibata et al. 2007; McConnachie et al. 2008; Richardson et al. 2011). Some of these systems have very well defined RGBs (e.g., And XIV, And XXI, And XXIII) while others have RGBs that are barely visible, with only ~20 stars (e.g., And XII, And XX, And XXII,

---

[15] In the case of the very large And XIX, we limit ourselves to a region within 12′ of the centroid to avoid clutter.
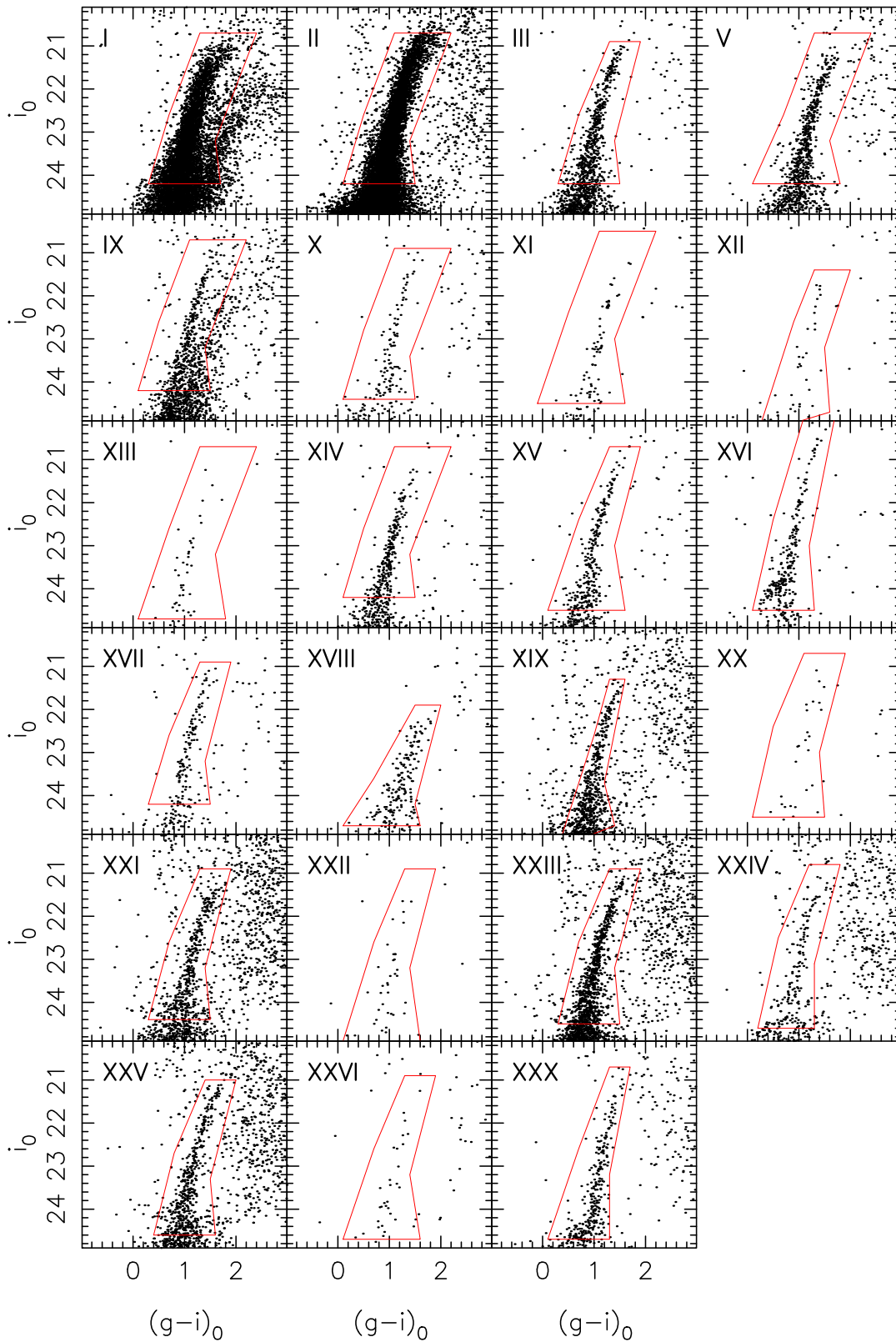
Figure 2. CMD of all M31 dwarf galaxies studied in this paper for a region within two half-light radii of a dwarf galaxy's centroid except for And XIX, for which the region has a smaller major axis of 12′. All dwarf galaxies show a more or less populated RGB, depending on the absolute luminosity of the system. The main contamination stems from red foreground dwarf stars that belong to the Milky Way disk or from nearby M31 halo stellar substructure in the case of And I and And IX. The polygons shown in red correspond to the CMD selection boxes used to isolate potential member stars on which the algorithms are ran.

And XXVI). The varying amount of contamination from foreground Milky Way stars is also evidence for the varying spatial extent of these systems. Finally, these dwarf galaxies are sometimes projected on other M31 halo stellar structures, which explains the complex RGB features present in the CMDs of And I and And IX that both overlap the metal-rich M31 Giant Stream or

its associated NE Shelf debris (Ibata et al. 2001; Ferguson et al. 2002; Fardal et al. 2007).

Figures 28–39, in Appendix A, show the spatial distribution of PAndAS stars in the regions used for the inference around each dwarf galaxy, along with the favored $2r_h$ region.

3. METHODS

3.1. Structure

The probability distribution functions (PDFs) of the dwarf galaxies' structural parameters are determined with an updated version of the M08 algorithm that now accounts for spatially incomplete data sets (such as the PAndAS observations that sometimes suffer from chip gaps and holes created by saturated foreground stars) and relies on Markov Chain Monte Carlo samplings of the posterior PDFs. We take this opportunity to describe this latest version of the algorithm.

For a sky region, $\mathcal{A}$, around a given dwarf galaxy, we work with a set of n CMD-selected PAndAS data points, $\mathcal{D}_n = \{d_k\}_{1 \leqslant k \leqslant n}$. Each datum is defined by its spatial coordinates on the sky, which can be simplified to the coordinates on the plane tangent to the sky at the dwarf galaxy's centroid assuming literature values,[16] $d_k = \{x_k, y_k\}$. The likelihood that these data points follow a specific radial density model, defined by the set of parameters $\mathcal{P} = \{p_1, p_2, ..., p_j\}$, is then defined as

$$P_{\text{tot}}(\mathcal{D}_n|\mathcal{P}) = \prod_k P_k(d_k|\mathcal{P}), \qquad (1)$$

where $P_k(d_k|\mathcal{P})$ is the likelihood of datum k to be generated from the chosen model. For the problem at hand, this likelihood can be expressed as the stellar surface density of the model, ρ_{model}, normalized to the number of stars expected to be in region $\mathcal{A}$. In other words,

$$P_k(d_k|\mathcal{P}) = \frac{\rho_{\text{model}}(d_k|\mathcal{P})}{\int_{\mathcal{A}} \rho_{\text{model}} d\mathcal{A}}. \qquad (2)$$

As described in M08, the family of radial density dwarf galaxy models at radius r, $\rho_{\text{model}}(r)$, is defined by an offset (x_0, y_0) of the centroid from the initial literature value, an ellipticity ϵ defined as $\epsilon = 1 - b/a$, with b/a the minor-to-major-axis ratio of the system, the position angle of the major axis θ, defined east of north, the half-light radius[17] of its assumed exponential radial profile, r_h, and the number of stars in the system for the chosen CMD selection,[18] N^*, such that

$$\rho_{\text{dwarf}}(r) = \frac{1.68^2}{2\pi r_h^2 (1-\epsilon)} N^* \exp(-1.68 r/r_h). \qquad (3)$$

Further assuming a constant contamination level,[19] Σ_b, around the studied stellar system yields

$$\rho_{\text{model}}(r) = \rho_{\text{dwarf}}(r) + \Sigma_b. \qquad (4)$$

In this equation, r is the elliptical radius, which relates to projected sky coordinates (x, y) via

$$r = \left\{ \left[\frac{1}{1-\epsilon}((x-x_0)\cos\theta - (y-y_0)\sin\theta) \right]^2 + [(x-x_0)\sin\theta + (y-y_0)\cos\theta]^2 \right\}^{1/2}. \qquad (5)$$

As in M08, we normalize the likelihood function by further enforcing that the model has the same number of stars in region $\mathcal{A}$, n, as is found in the PAndAS data, which sets the value of the background level,

$$\Sigma_b = \left(n - \int_{\mathcal{A}} \rho_{\text{dwarf}} d\mathcal{A} \right) \Big/ \int_{\mathcal{A}} d\mathcal{A}. \qquad (6)$$

Note that, contrary to M08, we do not assume that $\mathcal{A}$ is continuous. In effect, it can include regions with no data (chip gaps, bright stars, etc.), and, consequently, the integration of Equation (6) is performed numerically over a grid with pixels no larger than 5 times smaller than the inferred half-light radius.

Together, Equations (3)–(6) entirely define the likelihood of a data point as described in Equation (2) and, from there, the likelihood of the data given the model, P_{tot}, with Equation (1). Following Bayes's rule, $P_{\text{tot}}(\mathcal{D}_n|\mathcal{P})$ is proportional to what one is ultimately concerned with, $P(\mathcal{P}|\mathcal{D}_n)$, the probability of the model given the data, via multiplicative priors. Since the PAndAS data are generally powerful enough that any set of sensible priors yields similar results, we use flat priors for all parameters, making sure they nevertheless remain physical:

1. $0 \leqslant \epsilon < 1.0$,
2. θ included in an interval of 180°,
3. $0 < r_h \leqslant r_{\text{max}}$,
4. $N^* > 0$.

In most cases, $r_{\text{max}} = +\infty$, except for the faintest dwarf galaxies for which the algorithm can diverge and attempt to fit a model that is as wide as possible, which, in effect, means a simple increase of the contamination level and the suppression of the dwarf galaxy in the model. However, since we know from spectroscopy and deeper photometry that an M31 stellar overdensity is present in every field, we fix r_{max} to a value that is clearly larger than the size of the stellar overdensity in these few cases. This choice will be detailed in Section 4 when relevant.

Finally, we use a homemade, simple Metropolis–Hastings algorithm to sample the posterior distribution functions. The algorithm was typically run for hundreds of thousands of iterations to achieve visually appealing PDFs in the figures, which ensured convergence. The outcomes of the fits are

---

[16] Note that we infer updated centroid positions as two of the model parameters correspond to offsets from these literature values, which only serve as starting points.

[17] What we really determine here is the half-density radius since we study the distribution of stars on the sky, irrespective of their luminosity. However, under the assumption that a system harbors uniform stellar populations and does not suffer from mass segregation, this quantity is equivalent to the more common half-light radius. r_h is related to the exponential radius, r_e, by $r_h = 1.68 r_e$.

[18] For every dwarf galaxy, this CMD selection box is different and tailored around the visible RGB, as shown by the red polygons in Figure 2. It is wide enough in color to include all RGB stars, down to a depth that is usually above the horizontal branch (located around $i_0 \sim 25.0$ in most cases) so as not to be sensitive to field-to-field depth variations. The low density of faint dwarf galaxies like And XII, And XXII, or And XXVI forces us to dig deeper into the data, down to the faint limit. These dwarf galaxies also happen to be the smallest ones, which limits the impact of field-to-field variations since they are completely included in a given MegaCam field.

[19] In cases such as those of And X and XIX (Sections 4.6 and 4.15 below) for which there is suspicion of a nonuniform background due to M31 stellar halo substructures, we also tested the use of smoothly varying background models in the form $\Sigma_b = ax + by + cxy + d$, with a, b, and c parameters of the model and d determined via its normalization. However, it does not yield significantly better results than with a flat background and comes at the cost of a more flexible model that does not converge as easily without added priors. We therefore restrict ourselves to a simple, flat background model and warn the reader in case of doubt about this assumption.

Table 1
Derived Structural Parameters of the Dwarf Galaxies

Name	α (J2000)	δ (J2000)	ϵ	θ (deg)	r_h (arcmin)	r_h (pc)[a]
And I	$0^h45^m39^s7 \pm 0^s3$	$+38°02'15'' \pm 6''$	0.28 ± 0.03	30 ± 4	3.9 ± 0.1	815 ± 40
And II	$1^h16^m26^s8 \pm 0^s4$	$+33°26'07'' \pm 6''$	0.16 ± 0.02	31 ± 5	5.3 ± 0.1	965 ± 45
And III	$0^h35^m30^s9 \pm 0^s4$	$+36°29'56'' \pm 8''$	0.59 ± 0.04	140 ± 3	2.0 ± 0.2	405 ± 35
And V	$1^h10^m17^s5 \pm 0^s4$	$+47°37'42'' \pm 6''$	$0.26^{+0.09}_{-0.07}$	54 ± 10	$1.6^{+0.2}_{-0.1}$	345 ± 40
And IX	$0^h52^m53^s4 \pm 0^s7$	$+43°11'57'' \pm 8''$	$0.00^{+0.16}_{-0.00}$	41 ± 65	$2.0^{+0.3}_{-0.2}$	360^{+60}_{-50}
And X[b,c]	$1^h06^m35^s4 \pm 0^s6$	$+44°48'27'' \pm 10''$	$0.10^{+0.34}_{-0.10}$	30^{+20}_{-12}	$1.1^{+0.4}_{-0.2}$	210^{+70}_{-35}
And XI	$0^h46^m19^s7 \pm 0^s6$	$+33°48'10'' \pm 8''$	$0.19^{+0.28}_{-0.19}$	54 ± 30	0.6 ± 0.2	120^{+53}_{-44}
And XII[c]	$0^h47^m28^s3 \pm 1^s3$	$+34°22'38'' \pm 37''$	$0.61^{+0.16}_{-0.48}$	16^{+12}_{-36}	$1.8^{+1.2}_{-0.7}$	420^{+280}_{-200}
And XIII	$0^h51^m51^s0 \pm 0^s5$	$+33°00'16'' \pm 13''$	$0.61^{+0.14}_{-0.20}$	-20^{+9}_{-12}	$0.8^{+0.4}_{-0.3}$	130^{+80}_{-62}
And XIV	$0^h51^m35^s0 \pm 0^s5$	$+29°41'23'' \pm 10''$	$0.17^{+0.16}_{-0.17}$	-4 ± 14	1.5 ± 0.2	~265
And XV	$1^h14^m18^s3 \pm 0^s5$	$+38°07'11'' \pm 7''$	0.24 ± 0.10	38 ± 15	1.3 ± 0.1	230^{+35}_{-25}
And XVI	$0^h59^m30^s3 \pm 0^s4$	$+32°22'34'' \pm 4''$	0.29 ± 0.08	98 ± 9	1.0 ± 0.1	130^{+30}_{-15}
And XVII	$0^h37^m06^s3 \pm 0^s6$	$+44°19'23'' \pm 6''$	0.50 ± 0.10	110 ± 9	1.4 ± 0.3	285^{+55}_{-45}
And XVIII	$0^h02^m15^s6 \pm 0^s5$	$+45°05'28'' \pm 11''$	$0.03^{+0.28}_{-0.03}$	42^{+40}_{-84}	0.8 ± 0.1	265 ± 50
And XIX[b]	$0^h19^m34^s5 \pm 3^s0$	$+35°02'41'' \pm 53''$	$0.58^{+0.05}_{-0.10}$	34 ± 5	$14.2^{+3.4}_{-1.9}$	3065^{+935}_{-1065}
And XX	$0^h07^m30^s6 \pm 0^s4$	$+35°07'37'' \pm 6''$	$0.11^{+0.41}_{-0.11}$	90^{+20}_{-44}	$0.4^{+0.2}_{-0.1}$	90^{+35}_{-20}
And XXI	$23^h54^m47^s9 \pm 1^s6$	$+42°28'14'' \pm 20''$	$0.36^{+0.10}_{-0.13}$	139 ± 13	$4.1^{+0.8}_{-0.4}$	1005 ± 175
And XXII/Tri I	$1^h27^m40^s4 \pm 0^s6$	$+28°05'25'' \pm 7''$	$0.61^{+0.10}_{-0.14}$	114 ± 10	$0.9^{+0.3}_{-0.2}$	225 ± 75
And XXIII	$1^h29^m21^s0 \pm 0^s8$	$+38°43'26'' \pm 13''$	$0.41^{+0.05}_{-0.06}$	138 ± 5	5.4 ± 0.4	1190 ± 100
And XXIV	$1^h18^m32^s7 \pm 1^s8$	$+46°22'13'' \pm 18''$	$0.10^{+0.31}_{-0.10}$	90 ± 34	$2.6^{+1.0}_{-0.5}$	680^{+250}_{-140}
And XXV	$0^h30^m09^s9 \pm 0^s9$	$+46°51'41'' \pm 16''$	$0.03^{+0.16}_{-0.03}$	-16 ± 30	$2.7^{+0.4}_{-0.2}$	545^{+95}_{-65}
And XXVI[c]	$0^h23^m46^s3 \pm 1^s0$	$+47°54'43'' \pm 16''$	$0.35^{+0.33}_{-0.35}$	50 ± 90	$1.0^{+0.6}_{-0.5}$	150^{+140}_{-80}
Cas II/And XXX	$0^h36^m34^s6 \pm 0^s6$	$+49°38'49'' \pm 5''$	$0.43^{+0.10}_{-0.12}$	110 ± 9	1.5 ± 0.2	270 ± 50

Notes.
[a] Calculated using the posterior heliocentric distance PDFs calculated by Conn et al. (2012a).
[b] Substructure in the field may impact the structural parameters.
[c] Stricter priors were used to ensure convergence. See the text for more details.

presented later with a detailed discussion of the results for all 23 dwarf galaxies in the sample (Figures 5–27 and Section 4). The special case of And XXVII is discussed in Section 4.24. The structural parameter inferences are also summarized in tabular form in Table 1. The figures show the marginalized one-dimensional posterior PDFs for the six parameters of the inference. The favored parameters are measured as the modes of these one-dimensional PDFs, and uncertainties are bound by the values of the parameters for which the probability is 61% of the peak value.[20] The figures further show, for every dwarf galaxy, a comparison of the most probable exponential profile, compared to the data binned following the most probable centroid, ellipticity, and position angle.

It should, however, be emphasized that a truthful representation of the PDFs, including covariance between parameters and a proper sampling of the PDFs, is given in electronic form (see Appendix B) and distributed with this paper. Any analysis that wishes to use the results presented here should strive to use these outputs of the MCMC algorithm instead of the distribution moments summarized in Table 1.

Figure 3 presents the two-dimensional PDFs of all the parameters for a fainter (And XX) and a brighter (And XXI) galaxy in the sample. These plots reveal the typical correlations one might expect between the various parameters. Similar figures can easily be constructed from the provided chains for the other dwarf galaxies.

Deriving the physical half-light radius of the stellar systems from the angular half-light radius of the model requires an estimate of the distance to the dwarf galaxies. These have been determined homogeneously by Conn et al. (2012a) from the same PAndAS data set. Therefore, for each step of our MCMC chain, we randomly draw a distance from their heliocentric distance PDFs for the relevant dwarf galaxy and use this distance to calculate the physical half-light radius. This way, we fold in the distance uncertainties in our assessment of the physical sizes of the systems. Although this has the consequence of sometimes giving poor constraints (e.g., the physical r_h PDF of And XIV is double peaked because its distance PDF is double peaked), we favor the homogeneity of the measurements by using only PAndAS data. Nevertheless, since we also provide the angular sizes, it will be straightforward to recalculate the physical sizes from a future set of more accurate distances.

As a final note, we wish to point out that we chose exponential functions to characterize the radial density profile of the dwarf galaxies because these have been commonly used to characterize dwarf galaxies (starting from Faber & Lin 1983) and correspond to a generic phase of dwarf spheroidal evolution (e.g., Read & Gilmore 2005). In addition, they are easier to deal with analytically than the also common Plummer profile and are parameterized by one fewer parameter than King profiles, which leads to easier convergence. Moreover, neither of the three types of profiles actually accounts for the complexity of the brighter dwarf galaxies that often contain multiple stellar populations with different spatial distributions. This is commonly seen in the better known Milky Way dwarf
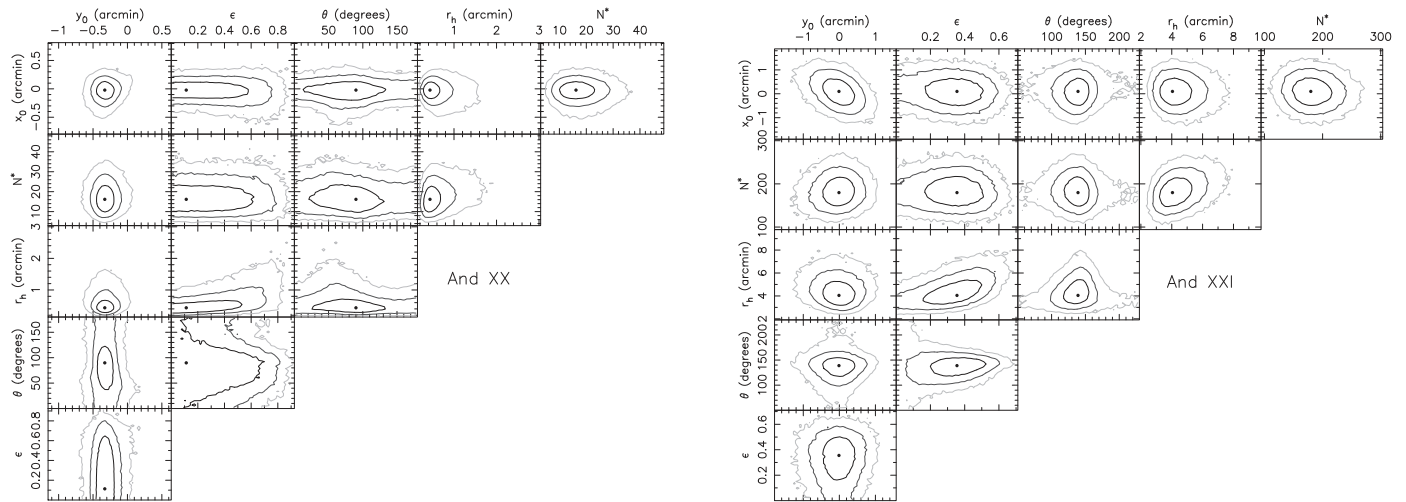
---

[20] This definition is equivalent to a $\pm 1\sigma$ deviation for a Gaussian distribution and mathematically equivalent to the commonly used "$\Delta\chi^2 = 1$" for such a distribution.

Figure 3. Two-dimensional PDFs of all the parameters for the And XX (left) and And XXI (right) inference. In each panel, the dot represents the favored model, whereas the contours correspond to 1σ, 2σ, and 3σ confidence intervals assuming Gaussian distributions. Of course, these are only indicative in the case of non-Gaussian distributions.

galaxies (e.g., Tolstoy et al. 2004) but has also been shown to be the case for And II, one of the most studied Andromeda companions (McConnachie et al. 2007; Ho et al. 2015). It remains that exponential profiles are a simple way to characterize dwarf galaxies, especially over a range of luminosity and, likely, stellar content, even if the latter is difficult to constrain for the fainter systems.

3.2. Absolute Magnitudes

One of the outcomes of the structural parameter fit is that we now have samplings of the PDF of the number of stars, N^*, that a dwarf galaxy hosts for the chosen CMD selection box, corrected for chip gaps and other holes in the data. In and of itself, N^* is not very meaningful since the selection boxes change with the dwarf galaxy, the distance to it, and the depth of the data in this particular region of the survey. This number can, however, be converted into the absolute magnitude of the dwarf galaxy by sampling an artificial CMD representative of the stellar system (M08). We use this methodology below to calculate the absolute magnitude of the dwarf galaxies after determining the (in)completeness function of the data at any location in the PAndAS survey.

3.2.1. The PAndAS Completeness Model

We start by determining the completeness function of the survey data in the region around And XIV, for which we have deep and wide Subaru/SuprimeCam data. These SuprimeCam data were observed on the night of 2009 August 22 as part of an ongoing program to gather deep photometric follow-up for all M31 dwarf galaxies discovered post-2004 with wide-field imagers on 8 m class telescopes (e.g., Brasseur et al. 2011b). The data comprise 3×400 s and 9×220 s dithered exposures in the SuprimeCam g and i bands, respectively, obtained under exquisite conditions (image quality $\sim 0\rlap{.}''4$).

The images are reduced and stacked, and the photometry is performed in the usual way, using a version of the CASU pipeline (Irwin & Lewis 2001) updated to work on Suprime-Cam data. The resulting photometric catalog is calibrated onto the PAndAS photometry, and the two leftmost panels of Figure 4 show a comparison of the PAndAS and SuprimeCam

CMDs for the region within $5'$ of And XIV's centroid; the SuprimeCam data are obviously much deeper than PAndAS.

After cross-identifying the PAndAS and the SuprimeCam catalogs over the full SuprimeCam footprint minus a small region near the center of And XIV that could suffer from crowding, and minus the chip gaps and the halos of bright stars that are present in either of the two data sets, we calculate the fraction, η, of SuprimeCam stellar-like objects[21] that are present in the stellar-like PAndAS catalog for a given magnitude bin.[22] These fractions are represented by the filled and open circles in the right panel of Figure 4 for the g and i bands, respectively. Note that we do not require an object to be observed in the two bands at this stage as we aim to build two independent g- and i-band completeness functions, which, when combined, will yield the completeness of the full CMD.

These completeness data points are used to constrain models of the form

$$\eta(m) = \frac{A}{1 + \exp\left(\frac{m - m_{50}}{\rho}\right)}, \qquad (7)$$

where m is either the g-band or the i-band magnitude. For the g band, we find that the favored values are $A = 0.94$, $m_{50} = 24.88$, and $\rho = 0.65$, whereas, for the i band, we get $A = 0.93$, $m_{50} = 23.88$, and $\rho = 0.74$. The curves in the right panel of Figure 4 represent these best models.

Since the depth of the data varies as a function of position in the survey, we further need to shift these completeness models to brighter/fainter magnitudes when the PAndAS data are shallower/deeper. In order to do so, we use the median magnitude of stars whose photometric uncertainties are in the range of 0.09–0.11, $m_{\rm ref}$, as a reference point (i.e., the local 10σ depth of the data). For a given MegaCam field k in PAndAS, the completeness model of the m band, with $m = g$ or i, therefore becomes $\eta(m + m_{\rm ref,XIV} - m_{\rm ref,k})$, where $m_{\rm ref,XIV}$ is the reference magnitude of the field that contains And XIV.

---

[21] Stellar-like objects have CASU classification flags of -1 or -2 in both the g- and i-band observations.
[22] By doing so, we assume that the SuprimeCam data are 100% complete.
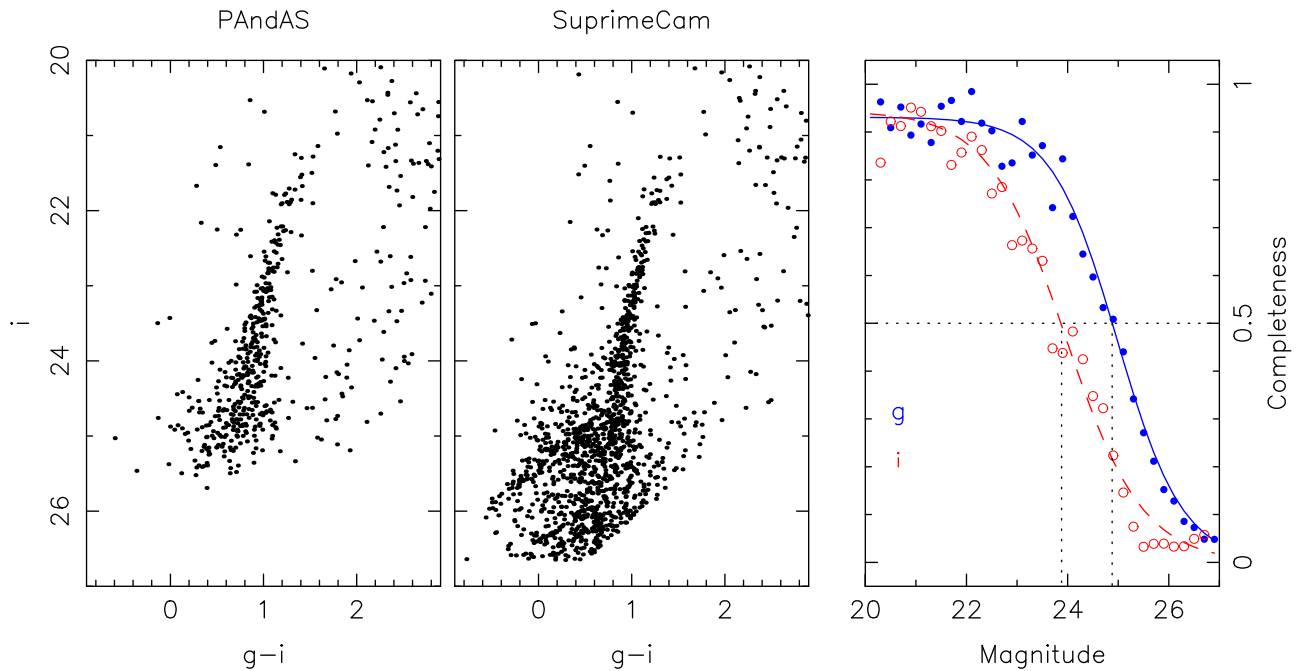
Figure 4. Comparison of the CMD of stars within 5′ of And XIV from PAndAS data (left) and from the SuprimeCam data used to derive the completeness function of the PAndAS data (middle). Neither of the two CMDs is dereddened. The right panel shows the fraction of SuprimeCam stars present in the PAndAS data for g-band magnitudes with blue filled circles and for i-band magnitudes with red open circles. The full blue line represents the best completeness model in the g band, as defined by Equation (7), while the dashed red line corresponds to the best model in the i band. The thin dotted lines indicate the values of 50% completeness, m_{50}.

An additional test with a shallower SuprimeCam field around And V yields model parameters that are consistent, within the uncertainties, with the model constrained on the And XIV data. We favor, however, the model built from And XIV as it corresponds to the deepest SuprimeCam data we have at our disposal.

3.2.2. Calculating M_V

For a given dwarf galaxy, we start by drawing a distance modulus from the distance MCMC chains of Conn et al. (2012a). We then model the PDF of its member stars in the CMD as a 13 Gyr PARSEC isochrone (Bressan et al. 2012) of the appropriate metallicity,[23] with the associated luminosity function (assuming the default Chabrier (2001) initial mass function), shifted to this distance modulus, reddened by the relevant amount of extinction measured from Schlegel et al. (1998) as recalibrated by Schlafly & Finkbeiner (2011), and convolved by the photometric uncertainties (see Martin et al. 2013a, for more details).[24] This model PDF is defined down to the hydrogen-burning limit.

A random drawing from the structural parameter MCMC chain of the dwarf galaxy yields the target N_i^* that we wish to

reproduce for a particular realization i of the dwarf galaxy's CMD. We then sample the color–magnitude PDF and flag sample stars that fall in the CMD selection box that was used to determine the structural parameters. We further randomly determine whether that star falls below both completeness functions for its g and i magnitudes and flag them accordingly. We repeat this process until we have accumulated N_i^* flagged stars. Summing up the flux of all the stars generated by this procedure (flagged or not) yields the apparent g-band and i-band magnitude of that realization of the dwarf galaxy, which we convert to the V band with the color equations given in Section 2.2 of Ibata et al. (2007) and correct for the extinction. In addition to the apparent magnitude, $m_{V,0}$, correcting from the distance modulus assumed earlier yields the V-band absolute magnitude, $M_{V,0}$, of this realization of the dwarf galaxy.

In order to account for uncertainties that stem from the (in) completeness model, we determine the impact on the And I magnitude values of varying the g- and i-band models by up to $\pm 1\sigma$ from the favored values determined in Section 3.2.1 above. These typically yield uncertainties of ± 0.2, and we therefore add a Gaussian random deviate of width 0.2 to the values of $m_{V,0}$ determined through the procedure above.

One may wonder about the impact of our choice of CMD selection boxes driving the uncertainties on N^* and, from there, those on $m_{V,0}$. Our framework naturally takes these into account as a wider and therefore more contaminated selection box will yield a more uncertain value for N^*, which will drive a more uncertain measure of the system's magnitude.

As we will see below, barring cases for which a direct comparison is not warranted (And XV, XVI, XVIII, and XIX), the revised magnitude values differ from the latest literature values by being, overall, 0.29 ± 0.11 mag fainter, which could be a consequence of our choice of a very old stellar population. New results show that (at least some) Andromeda dwarf
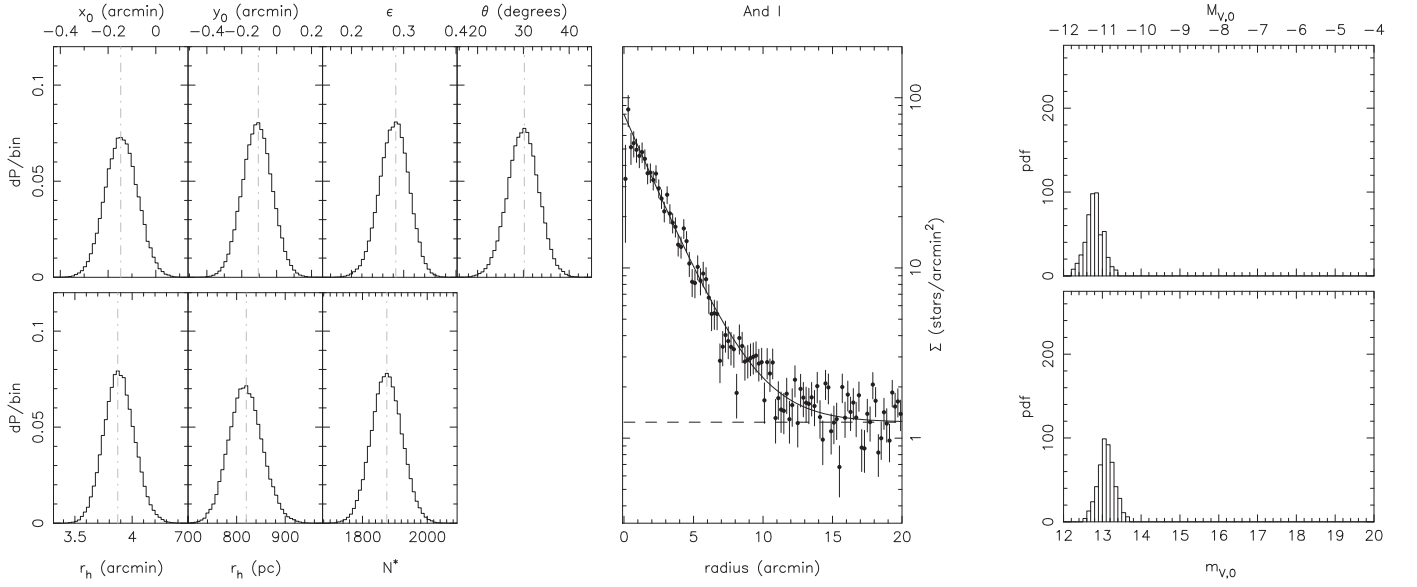
---

[23] Whenever possible, we use the spectroscopic metallicities compiled by Collins et al. (2013), with the exception of And I, for which we use the photometric metallicities derived by Kalirai et al. (2010), And II, for which we use the more recent spectroscopic value from Ho et al. (2015), and And X, for which we use the photometric metallicity derived by Brasseur et al. (2011a).

[24] As we did in Martin et al. (2013a), we further convolve the color–magnitude PDF of these single stellar populations with an additional, empirically determined 0.03 mag term that is added in quadrature to the photometric uncertainties. This has the consequence of producing slightly wider PDFs and accounts for the dwarf galaxies hosting more than single stellar populations. The impact of this widening is, however, almost insignificant in the current analysis.

Figure 5. Left: marginalized one-dimensional posterior PDFs for the structural parameter inference of And I. From top left to bottom right, the panels show the PDFs for the centroid (x_0, y_0), the ellipticity (ϵ), the position angle (θ), the angular and the physical half-light radii (r_h), and the mask-corrected number of stars that populate the dwarf galaxy within the chosen CMD selection box (N^*). The dashed vertical gray lines highlight the modes of the PDFs. Middle panel: comparison of the favored exponential radial density profile (solid line) with the PAndAS data binned in elliptical annuli following the favored structural centroid, ellipticity, position angle, and number of stars, corrected for regions of the survey that are masked out (dots, with the error bars representing Poisson uncertainties). The dashed line indicates the favored estimate of the flat background density (Σ_b). Right: PDF for the apparent and absolute magnitudes of And I (top and bottom, respectively).

Table 2
Derived Luminosity-related Properties of the Dwarf Galaxies

Name	$m_{V,0}$	$M_{V,0}$[a]	$\log_{10}(L_V/L_\odot)$[a]	μ_0 (mag arcsec^{-2})
And I	13.1 ± 0.2	-11.2 ± 0.2	6.38 ± 0.10	25.4 ± 0.2
And II	12.4 ± 0.2	-11.6 ± 0.2	6.54 ± 0.09	25.6 ± 0.2
And III	14.8 ± 0.2	-9.5 ± 0.3	5.68 ± 0.10	25.1 ± 0.3
And V	15.1 ± 0.2	-9.3 ± 0.2	5.61 ± 0.10	25.6 ± 0.3
And IX	15.6 ± 0.3	-8.5 ± 0.3	5.3 ± 0.1	26.7 ± 0.3
And X[b,c]	16.7 ± 0.3	-7.4 ± 0.3	4.9 ± 0.1	$26.6^{+0.6}_{-0.5}$
And XI	18.0 ± 0.4	$-6.3^{+0.6}_{-0.4}$	4.4 ± 0.2	26.8 ± 0.6
And XII[c]	17.7 ± 0.5	$-7.0^{+0.7}_{-0.5}$	4.7 ± 0.2	$28.7^{+0.7}_{-0.9}$
And XIII	17.8 ± 0.4	$-6.5^{+0.7}_{-0.5}$	$4.5^{+0.2}_{-0.3}$	26.6 ± 0.6
And XIV	15.8 ± 0.3	$-8.5^{+0.4}_{-0.3}$	$5.3^{+0.1}_{-0.2}$	26.3 ± 0.3
And XV	16.0 ± 0.3	$-8.0^{+0.3}_{-0.4}$	$5.1^{+0.2}_{-0.1}$	26.1 ± 0.3
And XVI	16.1 ± 0.3	-7.3 ± 0.3	4.8 ± 0.1	25.5 ± 0.3
And XVII	16.6 ± 0.3	-7.8 ± 0.3	5.0 ± 0.1	$26.4^{+0.4}_{-0.3}$
And XVIII	16.2 ± 0.4	$-9.2^{+0.3}_{-0.4}$	5.6 ± 0.2	$25.2^{+0.4}_{-0.5}$
And XIX[b]	14.5 ± 0.3	$-10.0^{+0.8}_{-0.4}$	$5.9^{+0.1}_{-0.3}$	29.3 ± 0.4
And XX	18.0 ± 0.4	$-6.4^{+0.5}_{-0.4}$	4.4 ± 0.2	25.8 ± 0.7
And XXI	15.5 ± 0.3	-9.1 ± 0.3	5.5 ± 0.1	28.0 ± 0.3
And XXII/Tri I	18.0 ± 0.4	$-6.7^{+0.7}_{-0.5}$	$4.6^{+0.2}_{-0.3}$	$26.9^{+0.6}_{-0.5}$
And XXIII	14.6 ± 0.2	$-9.8^{+0.2}_{-0.3}$	5.8 ± 0.1	27.5 ± 0.2
And XXIV	16.3 ± 0.3	-8.4 ± 0.4	5.3 ± 0.2	28.2 ± 0.4
And XXV	$15.3^{+0.3}_{-0.2}$	-9.0 ± 0.3	5.5 ± 0.1	27.1 ± 0.3
And XXVI[c]	$18.5^{+0.7}_{-0.5}$	$-5.8^{+0.9}_{-1.0}$	4.2 ± 0.4	28.0 ± 1.0
Cas II/And XXX	$16.0^{+0.3}_{-0.2}$	$-8.0^{+0.4}_{-0.3}$	5.1 ± 0.1	26.1 ± 0.3

Notes.
[a] Calculated using the posterior heliocentric distance PDFs calculated by Conn et al. (2012a).
[b] Substructure in the field may impact the structural parameters.
[c] Stricter priors were used to ensure convergence. See the text for more details.

galaxies contain a significant fraction of intermediate-age stars, younger than the 13 Gyr assumed above (Weisz et al. 2014c; Skillman et al. 2016). A test performed by assuming that And I is instead entirely composed of an 8 Gyr stellar population does lead to magnitudes that are systematically brighter by ∼0.2 mag. Without systematic star formation histories inferred
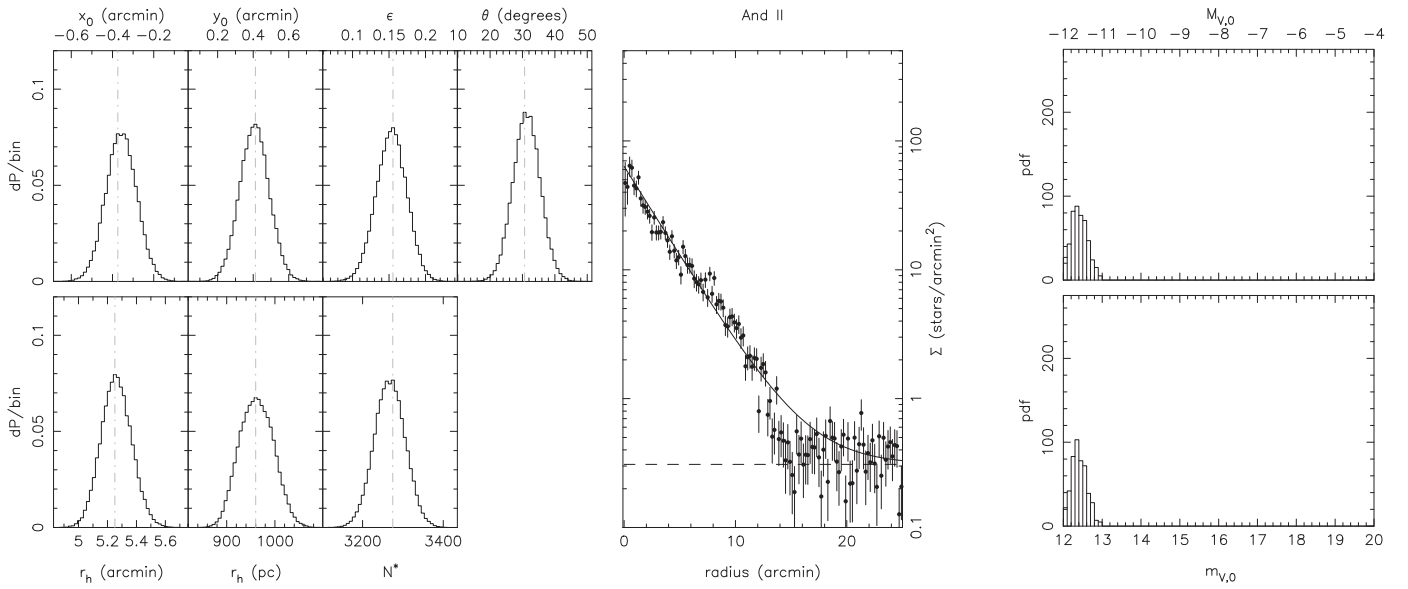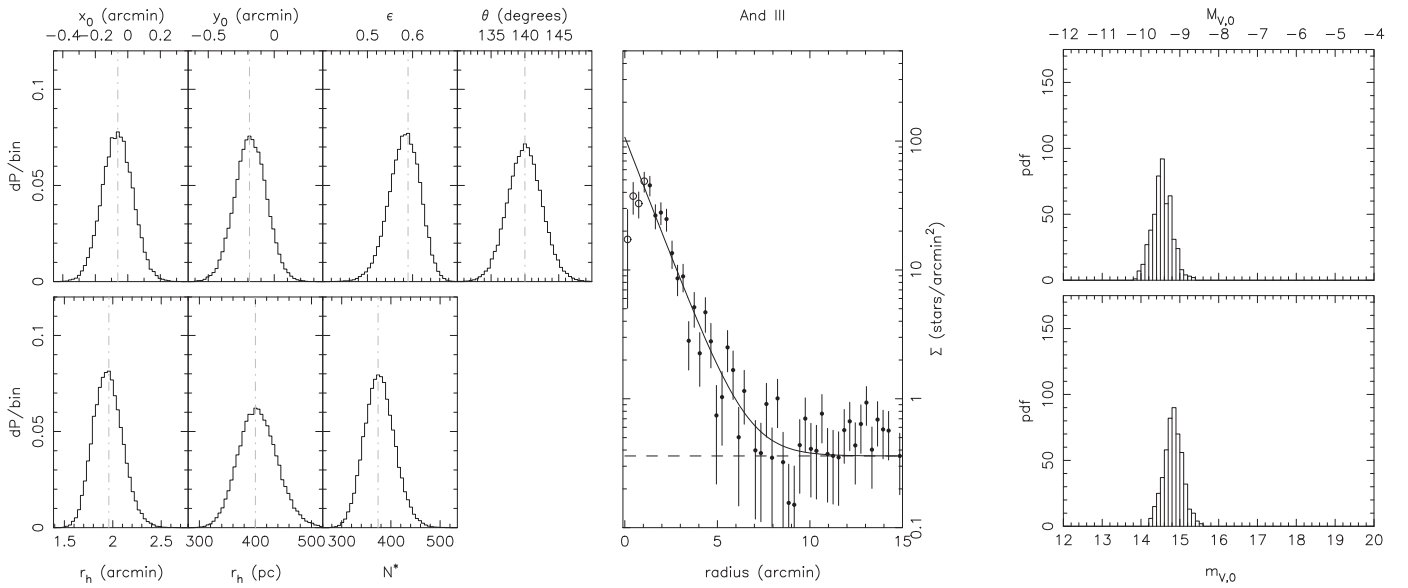
Figure 6. Same as Figure 5, but for And II.

Figure 7. Same as Figure 5, but for And III. In the middle panel comparing the radial density profile and the favored model, open circles represent regions affected by crowding that was not taken into account for the structural parameter inference.

from deep photometry for all the dwarf galaxies presented here, it is, however, too soon to use more complex stellar populations for the current study.

For every dwarf galaxy, we show the $m_{V,0}$ and $M_{V,0}$ PDFs resulting from 500 iterations of this procedure in the two rightmost panels of Figures 5–27. Table 2 summarizes the luminosity-related properties of the dwarf galaxies and lists the median of the distributions and the limits of their central 68% confidence interval. As for the structural parameters, we list random samples of the $m_{V,0}$ and $M_{V,0}$ PDFs in the MCMC chains distributed with this paper (see Appendix B).

3.3. Central Surface Brightness

Following Equation (6) of M08, the central surface brightness of a dwarf galaxy, $\mathcal{F}_0$, expressed in units of flux per

angular area, can be calculated as

$$\mathcal{F}_0 = \frac{\mathcal{F}}{2\pi r_e^2 (1 - \epsilon)}, \qquad (8)$$

where $\mathcal{F}$ is the total apparent flux of the system, which is easily calculated from the apparent magnitude $m_{V,0}$ determined in the previous section. The quantity $\mathcal{F}_0$ can then easily be transformed back into the more usual central surface brightness μ_0 expressed in mag arcsec^{-2}. These values are calculated for all dwarf galaxies, and every iteration of the chains and the resulting PDFs are summarized in Table 2.

4. RESULTS

This section presents the detailed comparison of our results for each dwarf galaxy with literature values from the latest

9
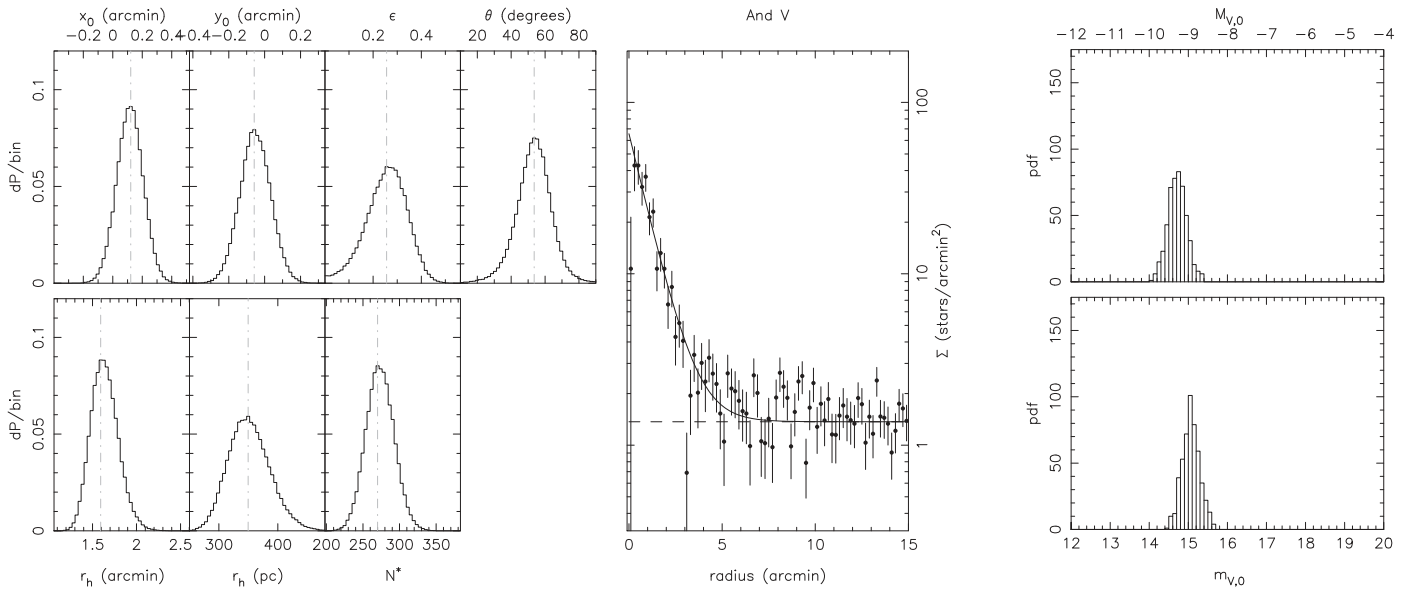
Figure 8. Same as Figure 5, but for And V.
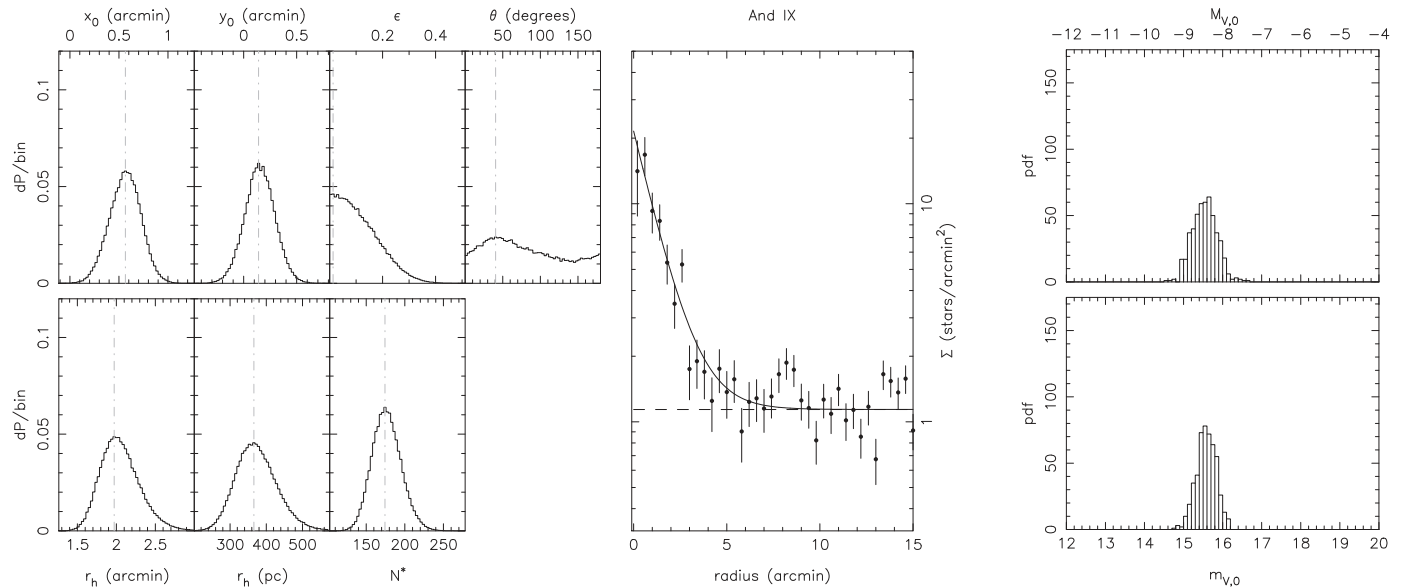
Figure 9. Same as Figure 5, but for And IX.

and/or deepest analyses. Whenever available, we will focus on the angular half-light radius and the apparent magnitude, as opposed to the physical half-light radius and the absolute magnitude since the latter parameters could be significantly affected by changes in the distance estimates. These were already covered in the detailed analysis of Conn et al. (2012a) that relied entirely on PAndAS data.

4.1. And I

And I is a bright dwarf galaxy that was initially discovered on photographic plates (van den Bergh 1972). The PDFs of the structural parameters we derive are all well behaved (left panels of Figure 5; $r_h = 3.9 \pm 0'.1$, $\epsilon = 0.28 \pm 0.03$, $m_{V,0} = 13.1 \pm 0.2$), the favored exponential model is entirely consistent with the data binned following the favored model (middle panel), and the magnitudes of this bright dwarf galaxy are very well

constrained due to the large number of stars on its RGB, which limits the impact of CMD "shot noise" (right panels).

The latest study of the structure of And I was performed by McConnachie & Irwin (2006) from INT/WFC data reaching ~1.5 mag below the dwarf galaxy's TRGB and yielded a fairly similar picture to the one presented here ($r_h = 2.9 \pm 0'.1$, $\epsilon = 0.22 \pm 0.04$, $m_{V,0} = 12.7 \pm 0.1$), albeit with some differences. However, the updated size of the system is significantly larger than before. This could be linked to the S-shaped outskirts of And I reported by McConnachie & Irwin (2006) and the deeper PAndAS data being more sensitive to tidally affected low surface brightness regions extending farther out. We also find that And I is slightly but significantly fainter than previously estimated, likely indicative of small systematics in either our or the INT/WFC study for cases such as this one where the RGB is very well populated and the CMD "shot noise" minimal.
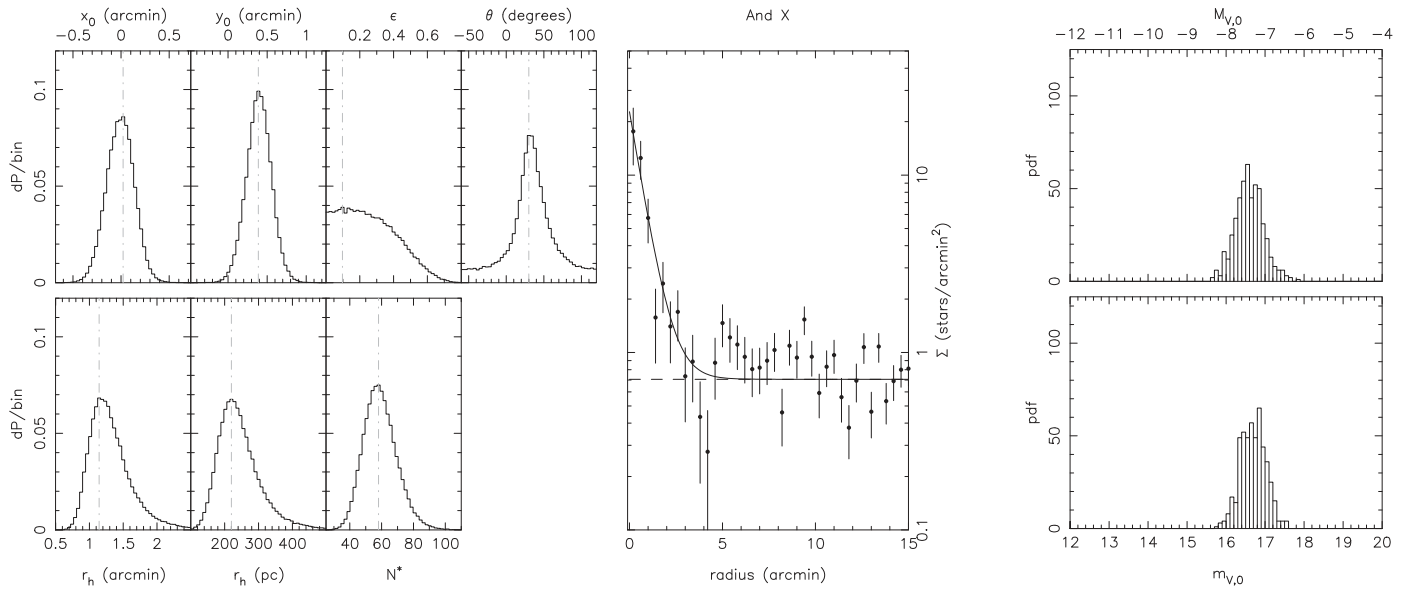
Figure 10. Same as Figure 5, but for And X.
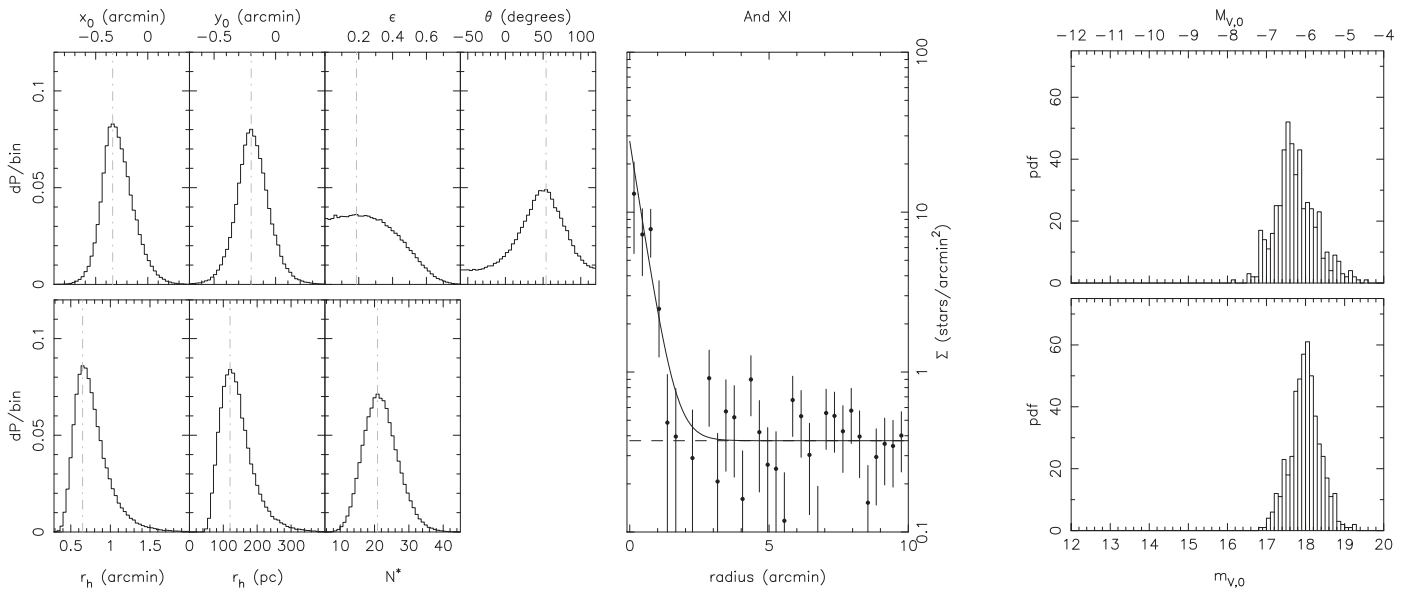
Figure 11. Same as Figure 5, but for And XI.

4.2. And II

And II was also discovered by van den Bergh (1972) from photographic plate studies. Its diagnostic plots are presented in Figure 6. As for And I, the PDFs are well behaved ($r_h = 5.3 \pm 0.'1$, $\epsilon = 0.16 \pm 0.02$, $m_{V,0} = 12.4 \pm 0.2$). However, the favored exponential profile shows discrepancies with the data binned following the favored model. This is not surprising as And II is known to host at least two distinct components with different chemistry and, more importantly, different radial density profiles (McConnachie & Irwin 2006; McConnachie et al. 2007; Weisz et al. 2014c). A recent study of RGB velocities further points to complex dynamics (Amorisco et al. 2014).

Our simple exponential radial density fit is evidently not an exact representation of this dwarf galaxy's properties, but it

nevertheless provides an easy way to compare And II with other, fainter dwarf galaxies that may also contain distinct stellar populations, even though they would likely escape detection. Our results are similar to the ones presented by McConnachie & Irwin (2006) from their shallower INT/WFC data ($r_h = 5.9 \pm 0.'1$, $\epsilon = 0.20 \pm 0.08$, $m_{V,0} = 11.7 \pm 0.2$).

4.3. And III

And III is much fainter than the previous two dwarf galaxies but was nevertheless found during the same analysis (van den Bergh 1972). The high central density of this fairly compact and reasonably bright dwarf galaxy leads to some crowding near its center in PAndAS. We consequently mask out an elliptical region of $1.'2$ when we infer the structural properties. The density estimates from this region are shown as open circles in
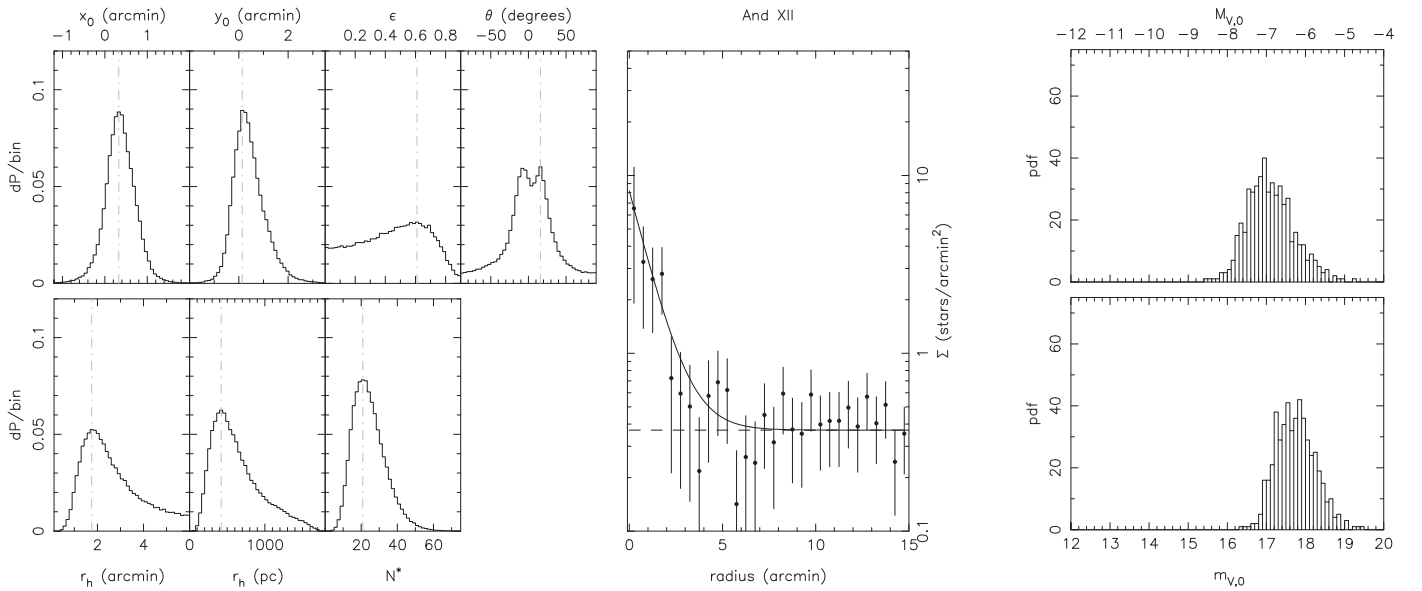
Figure 12. Same as Figure 5, but for And XII.
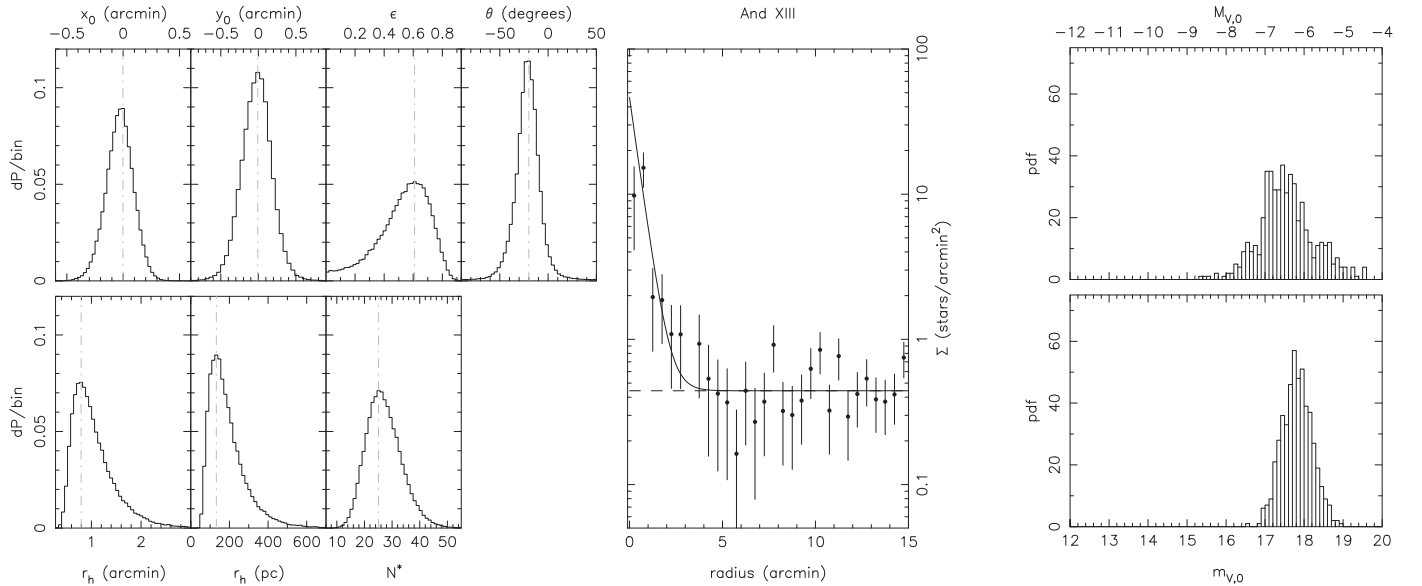
Figure 13. Same as Figure 5, but for And XIII.

the profile panel of Figure 7 ($r_h = 2.0 \pm 0'.2$, $\epsilon = 0.59 \pm 0.04$, $m_{V,0} = 14.8 \pm 0.2$). A chip gap also masks out a relatively large region in the densest parts of the dwarf galaxy (Figure 29), but the other panels of the figure nevertheless show well-behaved PDFs, and our results are consistent with those of McConnachie & Irwin (2006, $r_h = 1.7 \pm 0'.1$, $\epsilon = 0.52 \pm 0.02$, $m_{V,0} = 14.4 \pm 0.3$), once again from shallower INT/WFC imaging.

4.4. And V

And V was found in digitized photographic plates by Armandroff et al. (1998). Our results for this dwarf galaxy are presented in Figure 8 and paint a very similar picture to the one obtained for And III ($r_h = 1.6^{+0.2}_{-0.1}'$, $\epsilon = 0.26^{+0.09}_{-0.07}$, $m_{V,0} = 15.1 \pm 0.2$). Here as well, our results are consistent with those of McConnachie & Irwin (2006, $r_h = 1.4 \pm 0'.1$, $\epsilon = 0.18 \pm 0.05$, $m_{V,0} = 15.3 \pm 0.2$).

Overall, the comparison of our inference of the properties of the four bright Andromeda satellites And I, And II, And III, and And V with those from the INT/WFC analysis of McConnachie & Irwin (2006) shows good agreement, despite the two analyses being performed with completely different techniques and different data sets, thereby giving confidence in the current analysis before turning to fainter and less dense stellar systems.

Our results for And V are also very consistent with those of Collins et al. (2011) from Subaru/SuprimeCam data of similar depth to the PAndAS data ($r_h = 1.3 \pm 0'.1$, $\epsilon = 0.17 \pm 0.02$).

4.5. And IX

Figure 9 summarizes our results for the fainter And IX ($r_h = 2.0^{+0.3}_{-0.2}'$, $\epsilon = 0.00^{+0.16}_{-0.00}$, $M_{V,0} = -8.5 \pm 0.3$), which was found in the SDSS by Zucker et al. (2004). We infer a round system (explaining the poorly constrained position angle), with
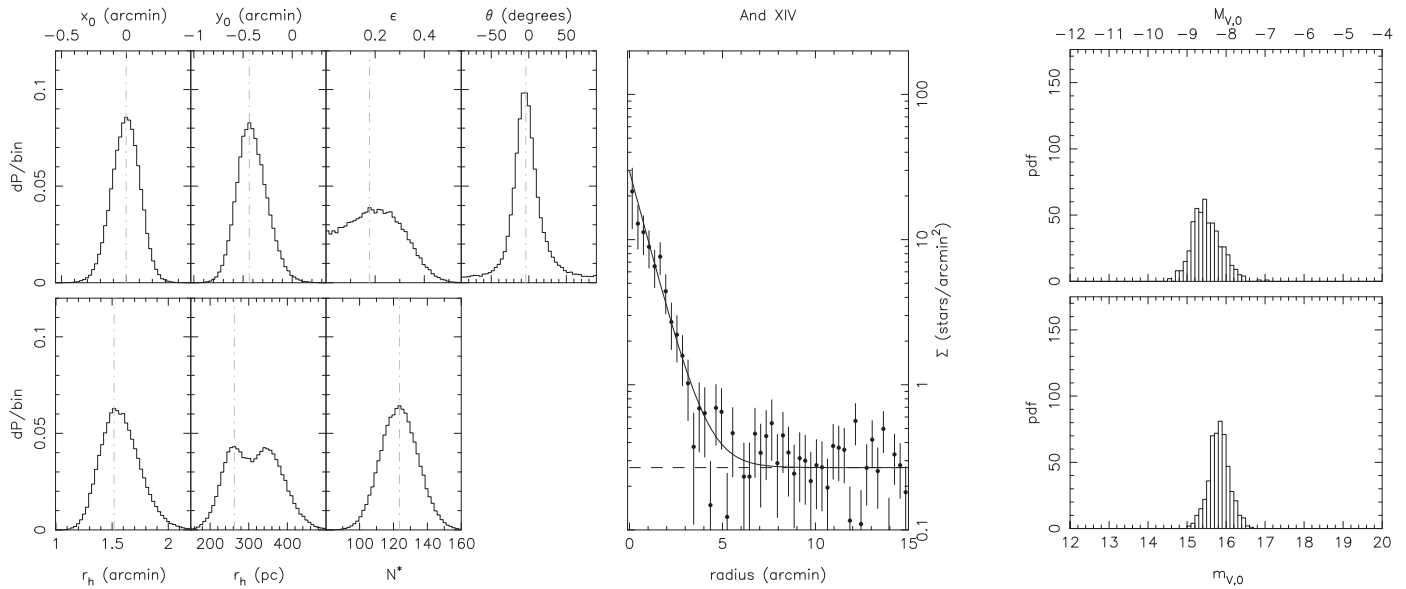
Figure 14. Same as Figure 5, but for And XIV.
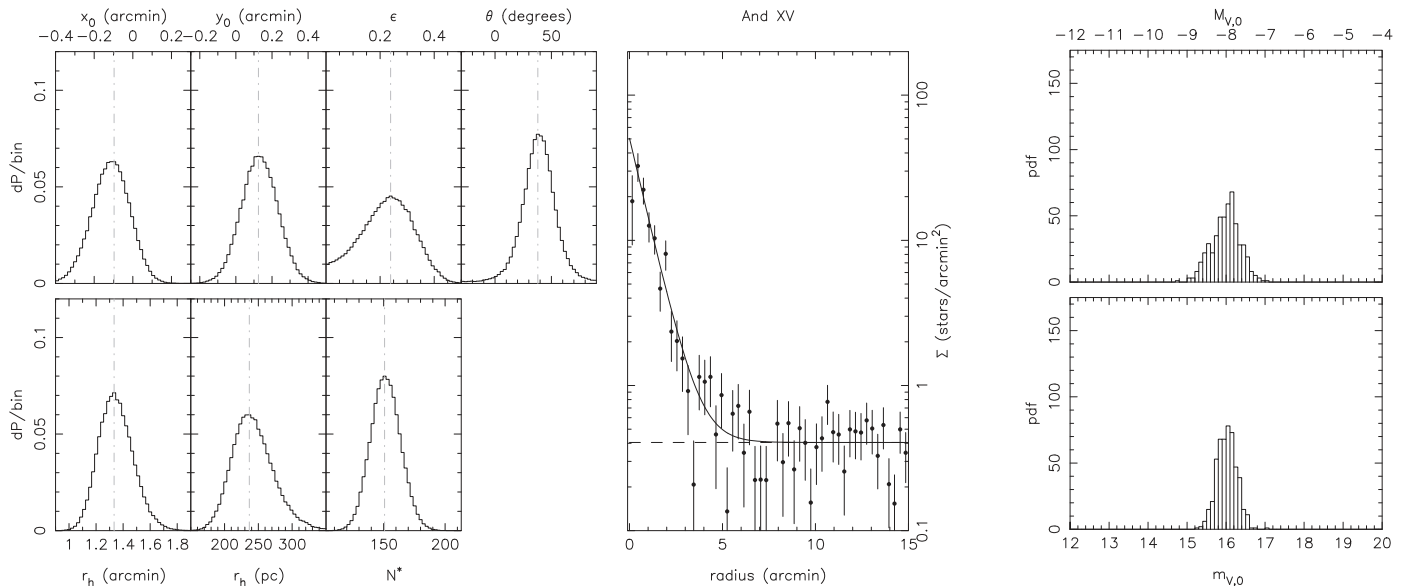
Figure 15. Same as Figure 5, but for And XV.

a smaller size compared to the previous inference from Subaru/SuprimeCam data of similar depth to the PAndAS data by Collins et al. (2010, assumption of circular symmetry, $r_h = 2.5 \pm 0.'1$, $M_{V,0} = -8.1^{+0.4}_{-0.1}$). It should, however, be noted that this previous analysis binned the data and relied on a smaller field of view, both of which can impact size estimates (M08; Muñoz et al. 2012). Our magnitude estimate is slightly brighter, although statistically consistent with that of the two previous analyses.

4.6. And X

The results for And X, discovered in the SDSS by Zucker et al. (2007), are summarized in Figure 10 ($r_h = 1.1^{+0.4}_{-0.2}'$, $\epsilon = 0.10^{+0.34}_{-0.10}$, $M_{V,0} = -7.4 \pm 0.3$) and are consistent with the structural parameters and magnitudes presented in Brasseur et al. (2011b) from LBC/LBT photometry that is deeper than the PAndAS data ($r_h = 1.3 \pm 0.'1$, $\epsilon = 0.44 \pm 0.06$,

$M_{V,0} = -7.4 \pm 0.9$). We find that And X is fairly round, but the uncertainties on our ellipticity inference fully include the larger and more accurate ellipticity measurement obtained from the LBC/LBT data with a method similar to the one described in this paper.

It should be noted that we enforced a stricter prior on the half-light radius, with $r_{max} = 6'$, to prevent a small fraction of the MCMC iterations from wandering off toward models with large r_h that clearly do not represent the structure of And X but likely track the structure in the field. And X lies in a region with some M31 halo stellar substructure, leading to a contamination level that is not perfectly flat.

4.7. And XI

And XI was discovered among the first set of pre-PAndAS MegaCam/CFHT observations (Martin et al. 2006) and later characterized in more depth by Collins et al. (2010). Our
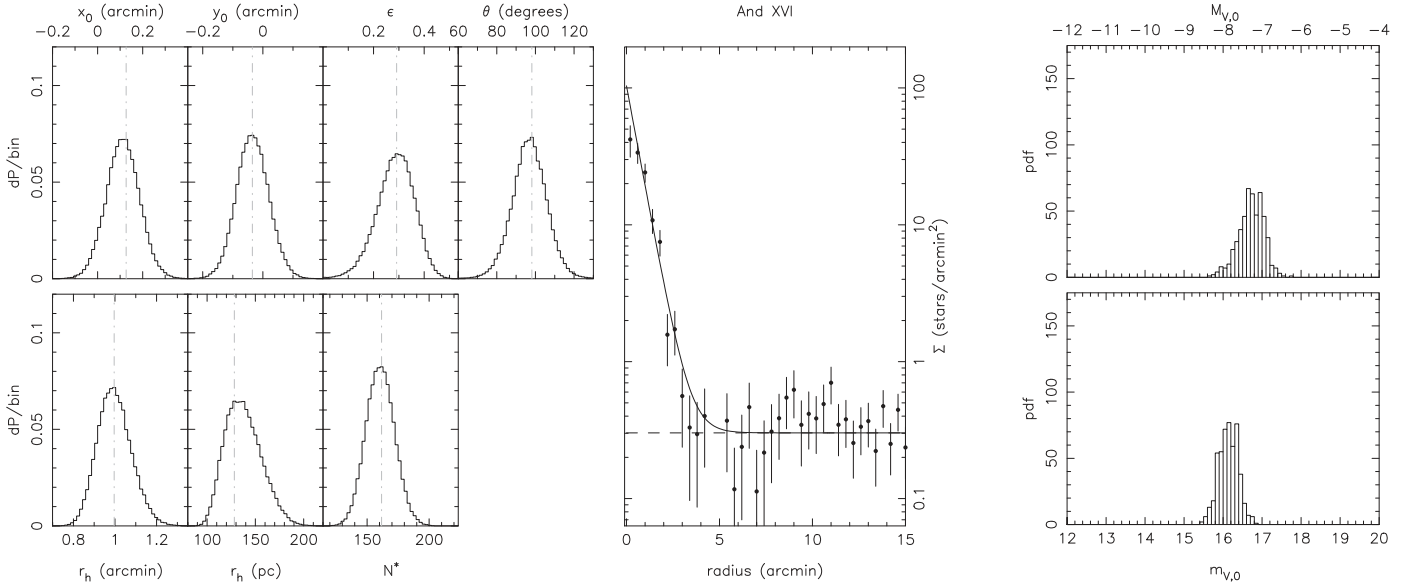
Figure 16. Same as Figure 5, but for And XVI.
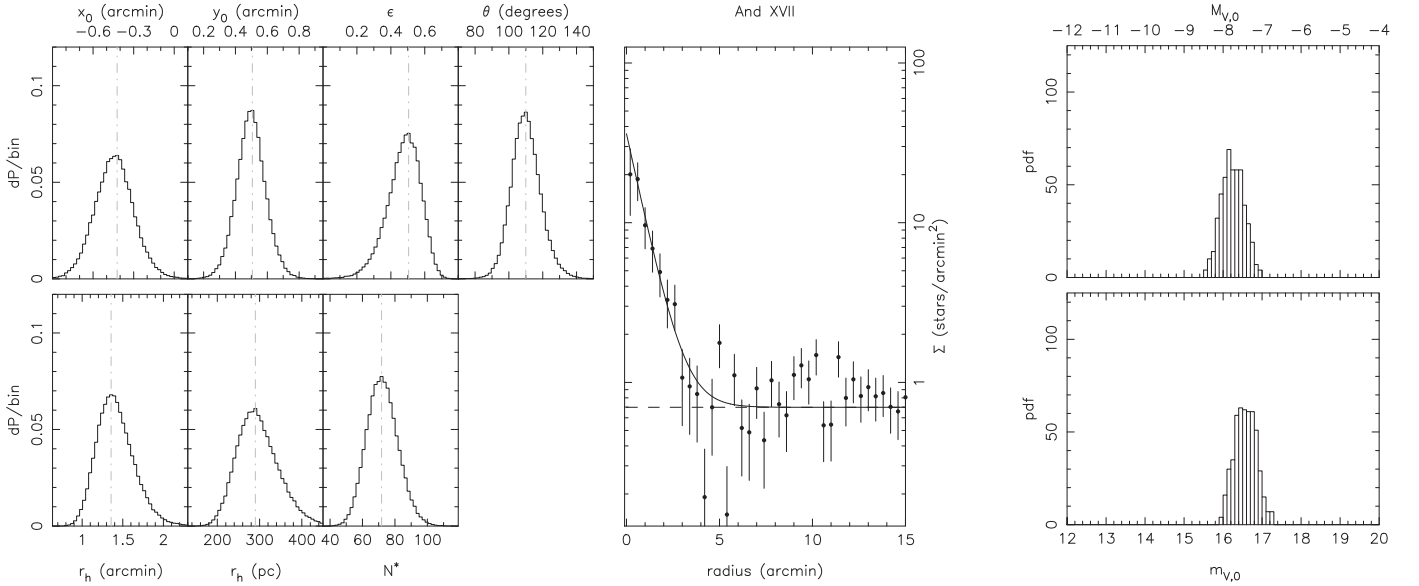
Figure 17. Same as Figure 5, but for And XVII.

results, summarized in Figure 11 ($r_h = 0.6 \pm 0.'2$, $\epsilon = 0.19^{+0.28}_{-0.19}$, $M_{V,0} = -6.3^{+0.6}_{-0.4}$), are consistent with those of the latter paper, based on Subaru/SuprimeCam data deeper than the PAndAS data (assumption of circular symmetry, $r_h = 0.7 \pm 0.'1$, $M_{V,0} = -6.9^{+0.5}_{-0.1}$). The width of the PDF for m_V highlights that CMD "shot noise" is important for this dwarf galaxy and must be taken into account.

4.8. And XII

Like And XI, And XII was discovered by Martin et al. (2006) and characterized more thoroughly from deeper Subaru/ SuprimeCam data by Collins et al. (2010, assumption of circular symmetry, $r_h = 1.1 \pm 0.'2$, $M_{V,0} = -6.4^{+0.1}_{-0.5}$). It is one of the faintest dwarf galaxies found around M31 and, as such, proves difficult to analyze with PAndAS data alone. This is reflected in the wide PDFs of Figure 12, in particular for the half-light radius

($r_h = 1.8^{+1.2}_{-0.7}'$, $\epsilon = 0.61^{+0.16}_{-0.48}$, $M_{V,0} = -7.0^{+0.7}_{-0.5}$). In addition, we were forced to use a stricter prior on this parameter ($r_{max} = 6.'0$) to prevent the chain from diverging. Despite these limitations, the PAndAS results are fully consistent with the results of Collins et al. (2010). CMD "shot noise" is once again significant for And XII.

4.9. And XIII

Like the previous two satellites, And XIII was discovered by Martin et al. (2006) and studied by Collins et al. (2010) from deeper SuprimeCam/Subaru photometry. Our conclusions, illustrated in Figure 13 ($r_h = 0.8^{+0.4}_{-0.3}'$, $\epsilon = 0.61^{+0.14}_{-0.20}$, $M_{V,0} = -6.5^{+0.7}_{-0.5}$), are fully consistent with those of the SuprimeCam analysis (assumption of circular symmetry, $r_h = 0.7 \pm 0.'1$, $M_V = -6.7^{+0.4}_{-0.1}$). CMD "shot noise" is significant for And XIII and at the same level as for And XI and
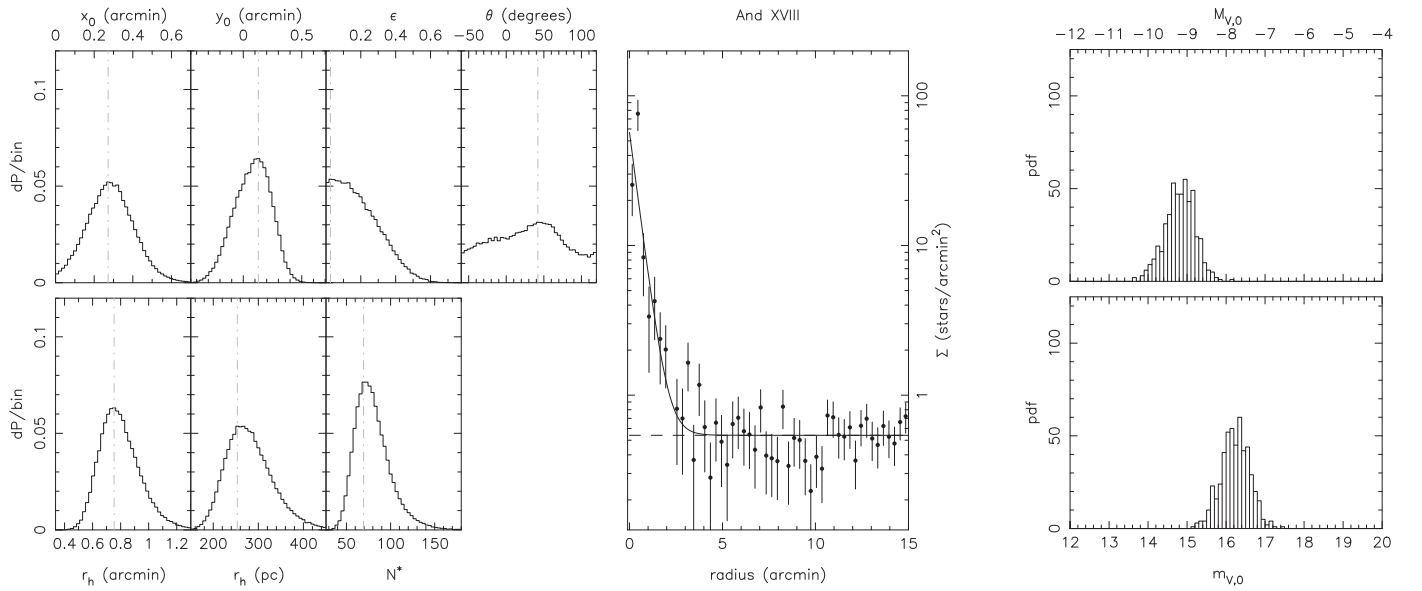
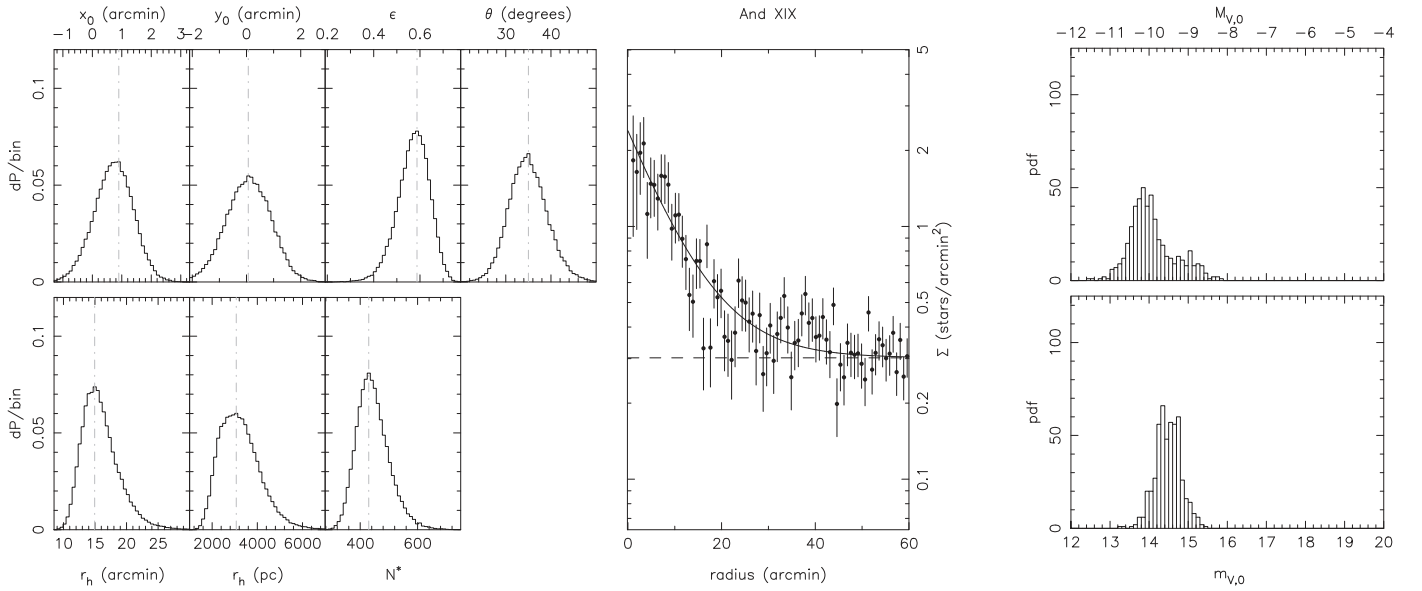**Figure 18.** Same as Figure 5, but for And XVIII.

Figure 19. Same as Figure 5, but for And XIX.

And XII. This is not surprising since these three dwarf galaxies share very similar properties, with $-7.0 \lesssim M_{V,0} \lesssim -6.3$.

4.10. And XIV

And XIV was serendipitously discovered by Majewski et al. (2007) before it was observed in PAndAS. For the analysis of this dwarf galaxy, we need to mask a large background galaxy and a bright foreground star, which, combined, represent a sizable fraction of the region within $2r_h$ of the centroid. And XIV is, however, dense enough that we derive good constraints on its structural parameters and magnitudes, as shown in Figure 14 ($r_h = 1.5 \pm 0.2'$, $\epsilon = 0.17^{+0.16}_{-0.17}$, $m_{V,0} = 15.8 \pm 0.3$). We are in very good agreement with the values of Majewski et al. (2007), recalculated by McConnachie (2012) for the parameters we use in our analysis

($r_h = 1.7 \pm 0.8'$, $\epsilon = 0.31 \pm 0.09$, $m_{V,0} \sim 15.9$). It should be noted that the complex distance modulus PDF Conn et al. (2012a) obtained for And XIV translates into complex physical r_h and M_V PDFs.

4.11. And XV

And XV was found within the pre-PAndAS MegaCam/CFHT data (Ibata et al. 2007), whose analysis assumed circular symmetry and yielded $r_h = 1.2 \pm 0.1'$ and $m_{V,0} = 14.3 \pm 0.3$. Our results (Figure 15) include the first inference of the ellipticity for this dwarf galaxy, which we find to be somewhat elliptical ($r_h = 1.3 \pm 0.1'$, $\epsilon = 0.24 \pm 0.10$, $m_{V,0} = 16.0 \pm 0.2$). The apparent magnitude we derive is significantly fainter than that of Ibata et al. (2007) and is not related to their assumption of spherical symmetry since values of N^* only increase by ~10% if
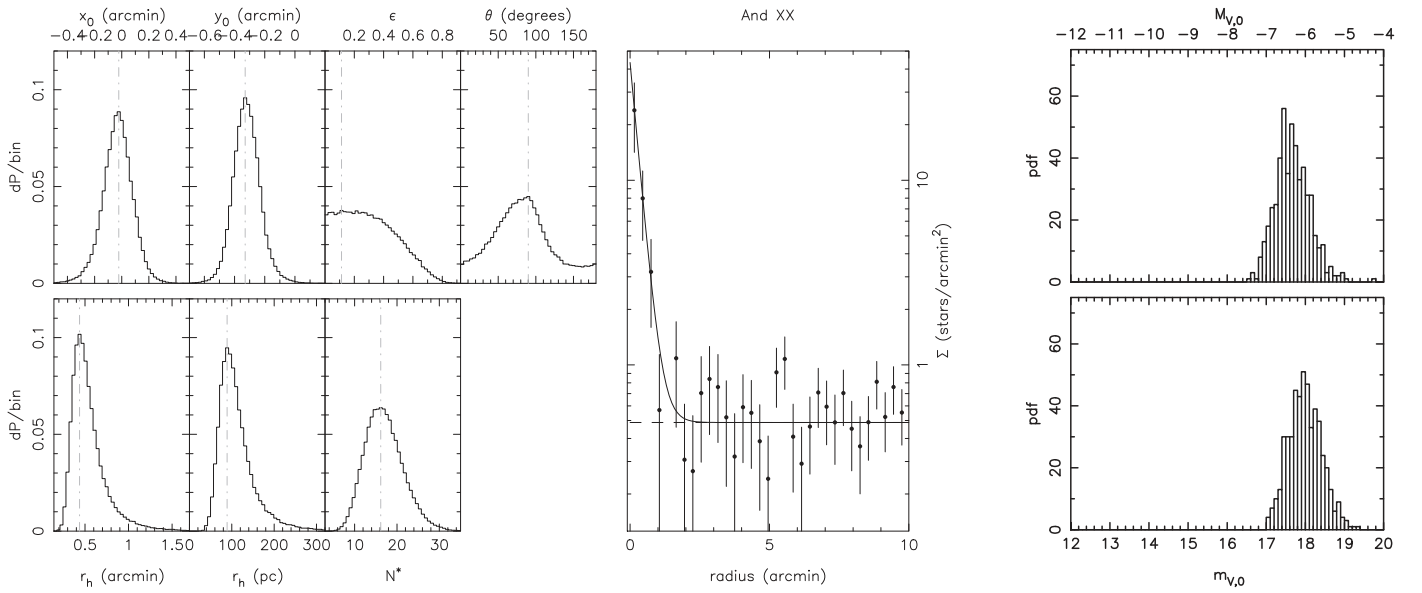
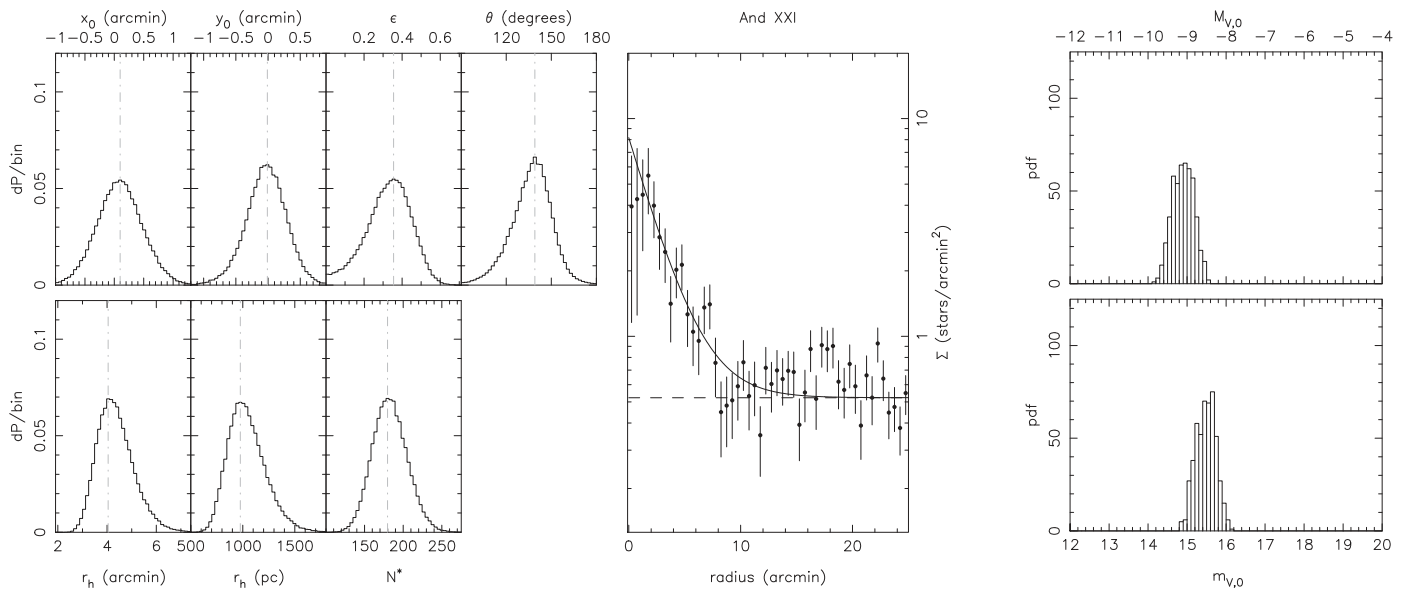**Figure 20.** Same as Figure 5, but for And XX.

Figure 21. Same as Figure 5, but for And XXI.

we enforce a circular model. A comparison of And XV's CMD with those of And IX and And X (Figure 2), all three located at similar distances ($24.0 < m - M < 24.4$; Conn et al. 2012a), shows that the RGB of And XV has a density bracketed by those of the two other dwarf galaxies. Therefore, their magnitudes should also bracket that of And XV; this is indeed what we find. The value from Ibata et al. (2007) would make And XV brighter than And III or And V, which is clearly not supported by Figure 2. This implies a flaw in our previous analysis, the origin of which we discuss next.

4.12. And XVI

Like And XV, And XVI was discovered in the pre-PAndAS MegaCam/CFHT study by Ibata et al. (2007), and, as before,

the structural parameters we infer ($r_h = 1.0 \pm 0\!'.1$, $\epsilon = 0.29 \pm 0.08$) are compatible with the one they derive, despite their assumption of circular symmetry ($r_h = 0.9 \pm 0\!'.1$). However, our estimate of the apparent magnitude of the dwarf galaxy is, again, significantly fainter ($m_{V,0} = 16.1 \pm 0.3$ versus 14.4 ± 0.3). Because And XVI is much closer to us ($m - M = 23.6 \pm 0.2$), the comparison of its CMD with those of other dwarf galaxies is made harder by the presence of And XVI's horizontal branch in Figure 2. With this in mind and focusing on the brighter regions of the RGB, And XVI appears to have a slightly lower number of RGB stars than And XV, closer to what is seen for And X. This visual comparison is in full agreement with our magnitude estimates for the three dwarf galaxies once we account for the differences in distance ($M_{V,0}^{XV} = -8.0_{-0.4}^{+0.3} < M_{V,0}^{XVI} = -7.3 \pm 0.3 \simeq M_{V,0}^{X} = -7.4 \pm 0.3$).
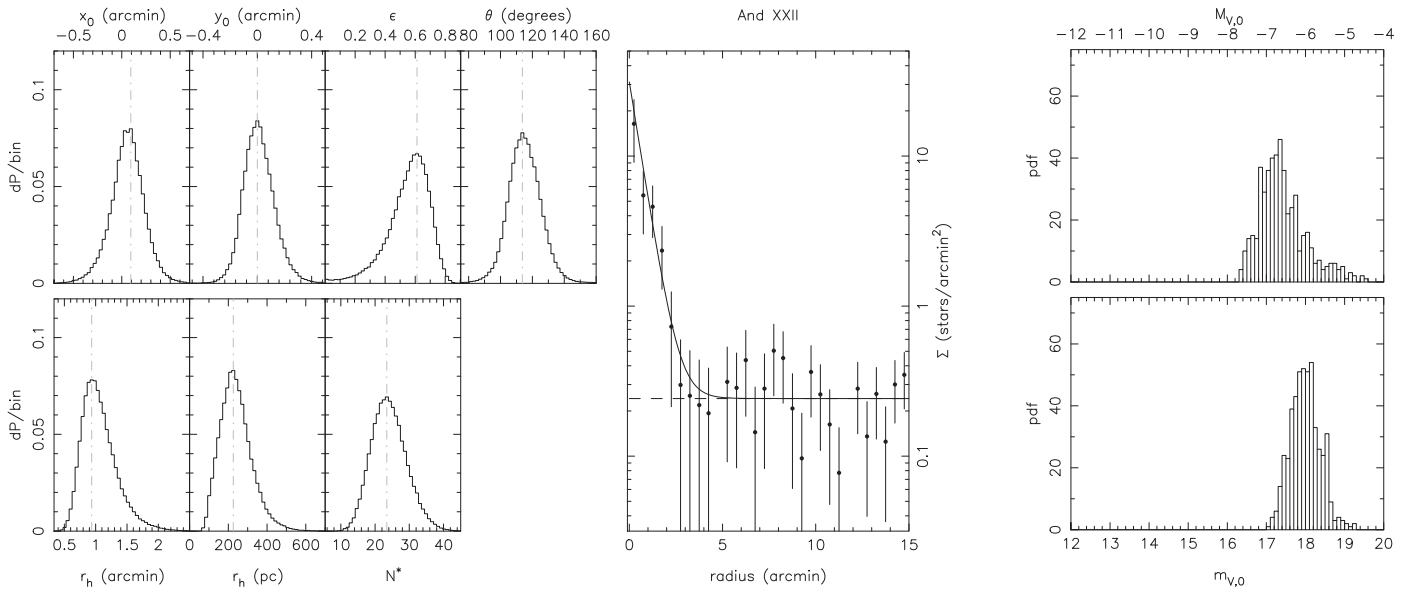
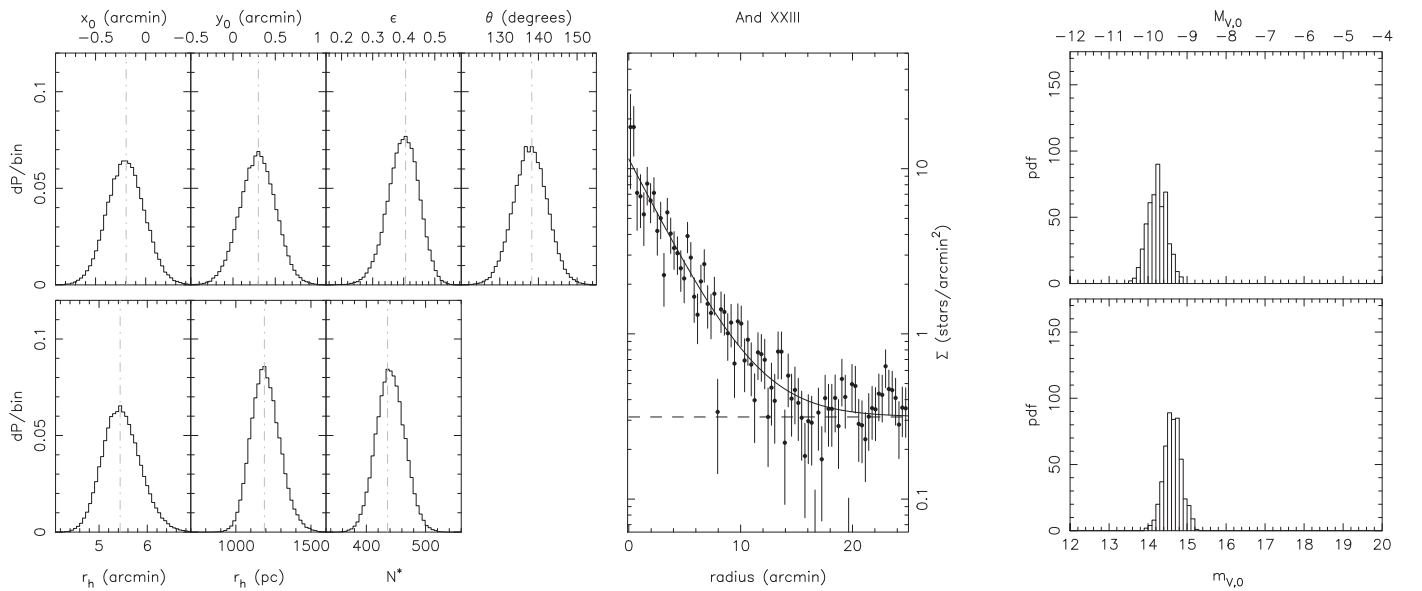**Figure 22.** Same as Figure 5, but for And XXII.

Figure 23. Same as Figure 5, but for And XXIII.

Ibata et al. (2007) derived the magnitudes of And XV and And XVI via their stellar counts within the region limited by r_h and by comparison with the same measurement applied to And III. An investigation of the details of the analysis, however, reveals that we did not account for the crowding at the center of And III or the significant PAndAS chip gap near the center of the dwarf galaxy (Figure 29), which likely led us to significantly underestimate the stellar counts within r_h for And III in the original analysis. This erroneously led us to conclude that And XV and And XVI had similar magnitudes to And III when they are in fact both much fainter.

This effect is now corrected in the new results, which give the picture of a fairly elliptical and faint dwarf galaxy (Figure 16).

4.13. And XVII

Discovered in an INT/WFC survey of the inner regions of the M31 halo (Irwin et al. 2008), And XVII was later studied in more detail by Brasseur et al. (2011b, $r_h = 1.2 \pm 0.1$, $\epsilon = 0.27 \pm 0.06$, $m_{V,0} = 15.8 \pm 0.4$) with LBC/LBT imaging that is deeper than the PAndAS data. Our results are shown in Figure 17 ($r_h = 1.4 \pm 0.3$, $\epsilon = 0.50 \pm 0.10$, $m_{V,0} = 16.6 \pm 0.3$). Although our size estimate agrees with the one based on the LBC data measured with a similar technique, our ellipticity is larger than before, and we derive a fainter apparent magnitude. A comparison of the CMD of And XVII with that of And XV seems to favor And XVII being at most as bright as And XV and therefore supports our magnitude measurement. It remains unclear, however, why our ellipticity measurement is $\sim 2\sigma$
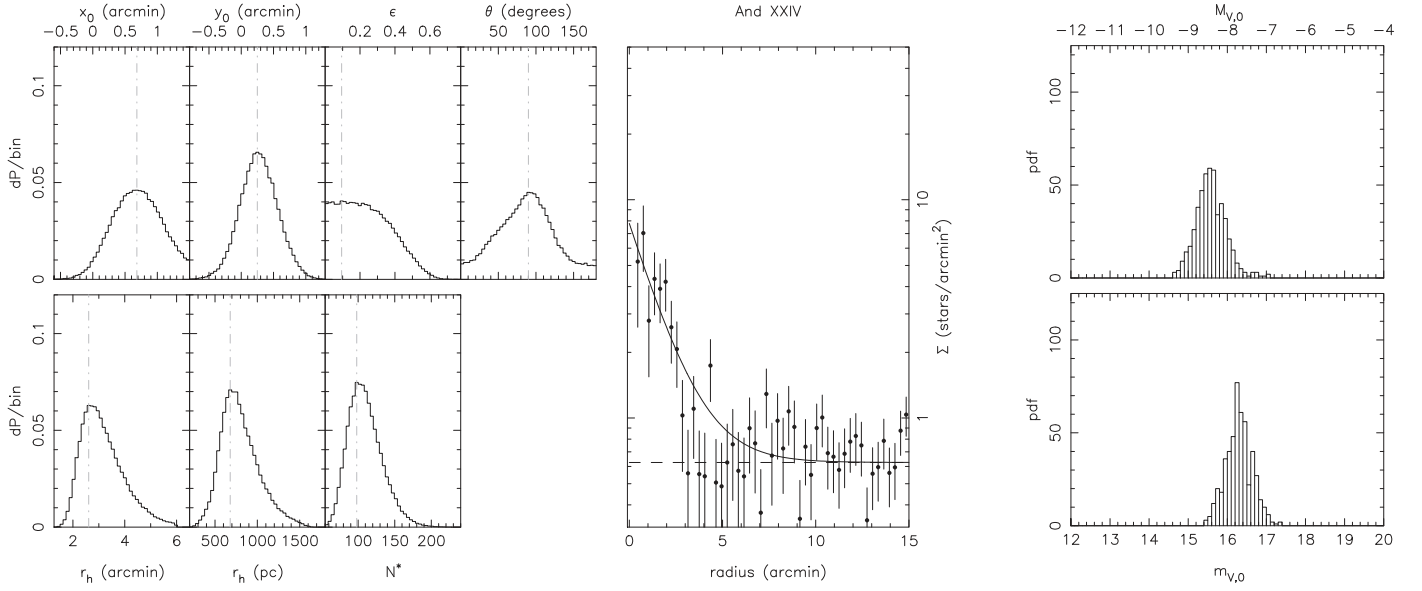
17

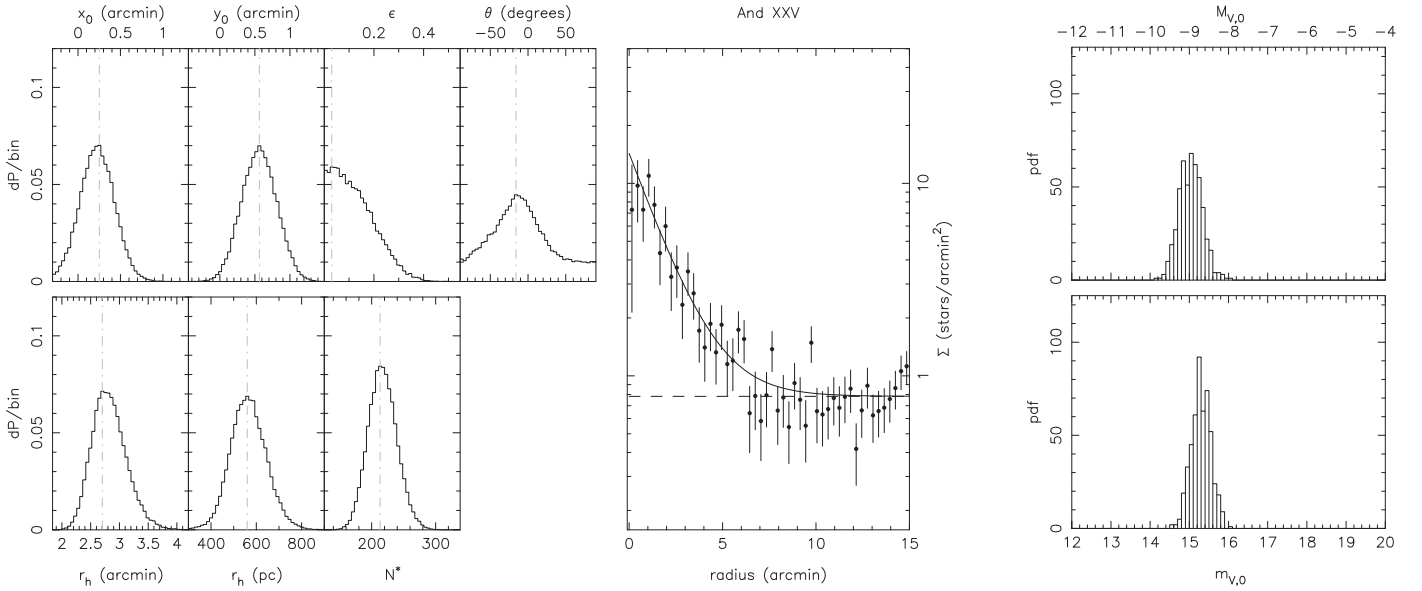**Figure 24.** Same as Figure 5, but for And XXIV.

Figure 25. Same as Figure 5, but for And XXV.

discrepant with the literature value. It could be related to Brasseur et al. (2011b) only using a much smaller spatial region for their analysis than we do here, which could potentially bias their results (Muñoz et al. 2012).

4.14. And XVIII

And XVIII was found in another batch of pre-PAndAS MegaCam/CFHT data by McConnachie et al. (2008). This previous analysis differs from the current one in its assumption of circular symmetry in order to cope with half of the dwarf galaxy overlapping a large chip gap (Figure 34), and it only provided a faint limit to the system's magnitude for the same reason ($r_h = 0.9 \pm 0.1$, $m_{V,0} \leqslant 16.0$). We do without this assumption here and rely on the masking of this region to derive the global structural properties of And XVIII ($r_h = 0.8 \pm 0.1$, $\epsilon = 0.03^{+0.28}_{-0.03}$, $m_{V,0} = 16.2 \pm 0.4$). Although the ellipticity is not well constrained, our size estimate is fully compatible with that found by McConnachie et al. (2008), and we can finally derive the dwarf galaxy's apparent magnitude, which, combined with its large distance behind M31 ($m - M = 25.42 \pm 0.08$; Conn et al. 2012a), implies that And XVIII is a fairly bright M31 satellite ($M_{V,0} = -9.2^{+0.3}_{-0.4}$). Our results are summarized in Figure 18.

4.15. And XIX

And XIX was also found by McConnachie et al. (2008) in pre-PAndAS MegaCam/CFHT data. Our results, presented in Figure 19 ($r_h = 14.2^{+3.4}_{-1.9}$, $\epsilon = 0.58^{+0.05}_{-0.10}$, $m_{V,0} = 14.5 \pm 0.3$),
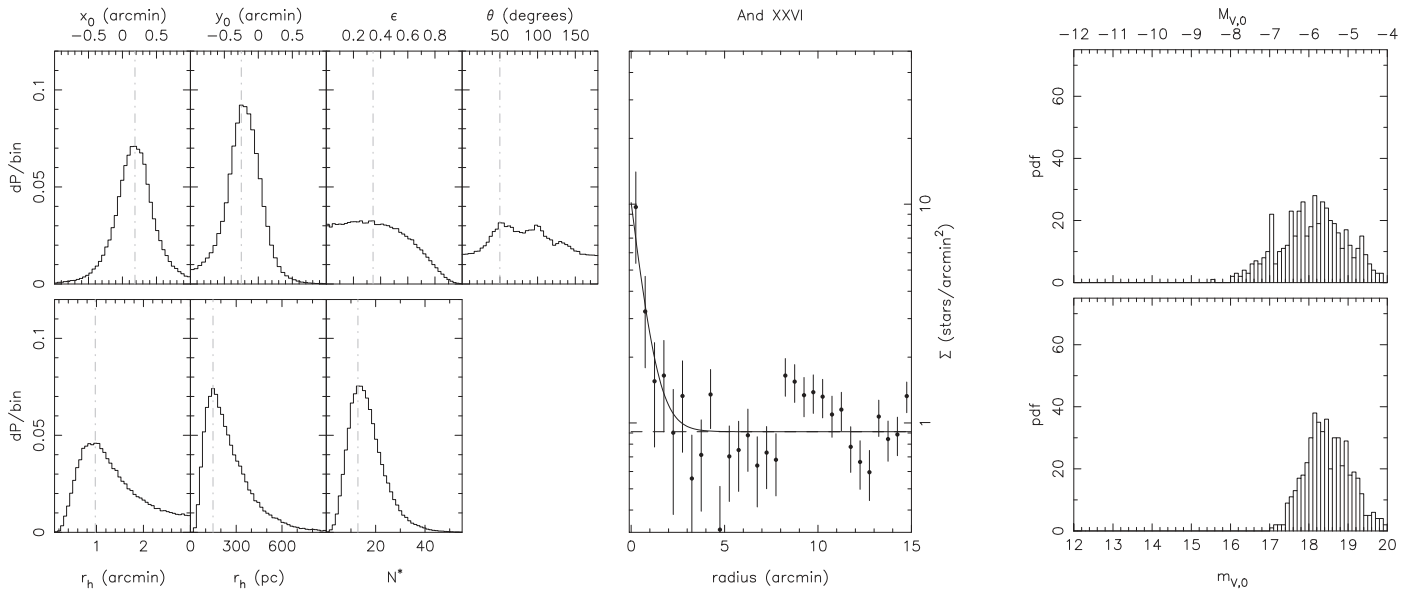
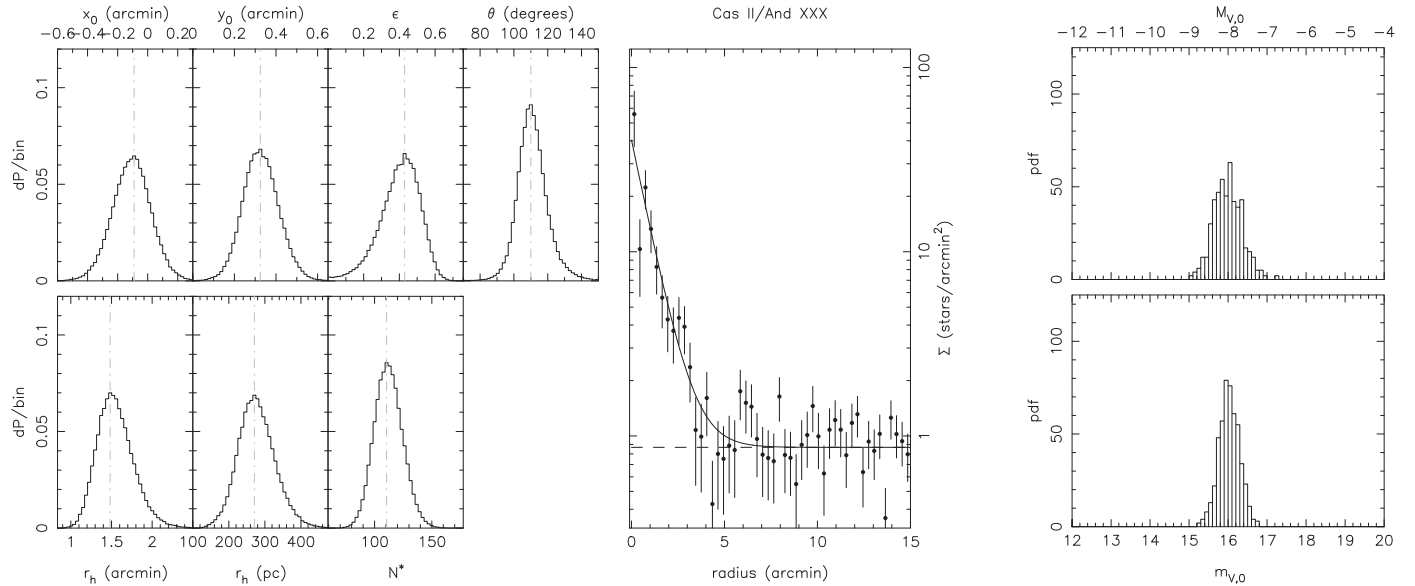**Figure 26.** Same as Figure 5, but for And XXVI.

Figure 27. Same as Figure 5, but for Cas II/And XXX.

differ drastically from the literature values ($r_h = 6.2 \pm 0'.1$, $\epsilon = 0.17 \pm 0.02$, $m_{V,0} = 15.6 \pm 0.6$), which we derived from what now clearly appears as a spatial region of the survey that was much too small for the analysis of this dwarf galaxy. This led to the much smaller half-light radius (see also Muñoz et al. 2012, for the impact of using a small field of view to derive the size of a dwarf galaxy). In the current analysis, we use a sample that extends $\pm 70'$ away from And XIX's centroid, leading to the inference of a much larger system. The fact that we also find And XIX to be very elliptical implies that the stellar stream it is embedded in (McConnachie et al. 2008; see also Figure 2 of Bate et al. 2014) further impacts our results and may be responsible for the positive counts above the favored radial density profile at $\sim 40'$ (middle panel of Figure 19). In addition, the large extent of the region considered means that the assumption of a flat background is

likely an approximation to the true stellar density in the chosen CMD selection box.

With a half-light radius as large as $14.2^{+3.4}_{-1.9}{}'$ or 3065^{+935}_{-1065} pc, it is uncertain whether And XIX can still be classified as a dwarf galaxy or whether it is so disrupted that its properties cannot be directly compared to other pristine dwarf galaxies. The only Local Group dwarf spheroidal galaxy with a similar size is Sagittarius (Majewski et al. 2003), which is clearly being pulled apart by gravitational tides. Alternatively, And XIX could be a fainter and local counterpart of the "extremely diffuse" galaxies recently found in the Coma Cluster (van Dokkum et al. 2015). Ultimately, a detailed spectroscopic analysis of the system's kinematics, developing the initial analysis of Collins et al. (2013) over the large body of the system, is mandatory to understand the state of And XIX and whether it remains a bound system.
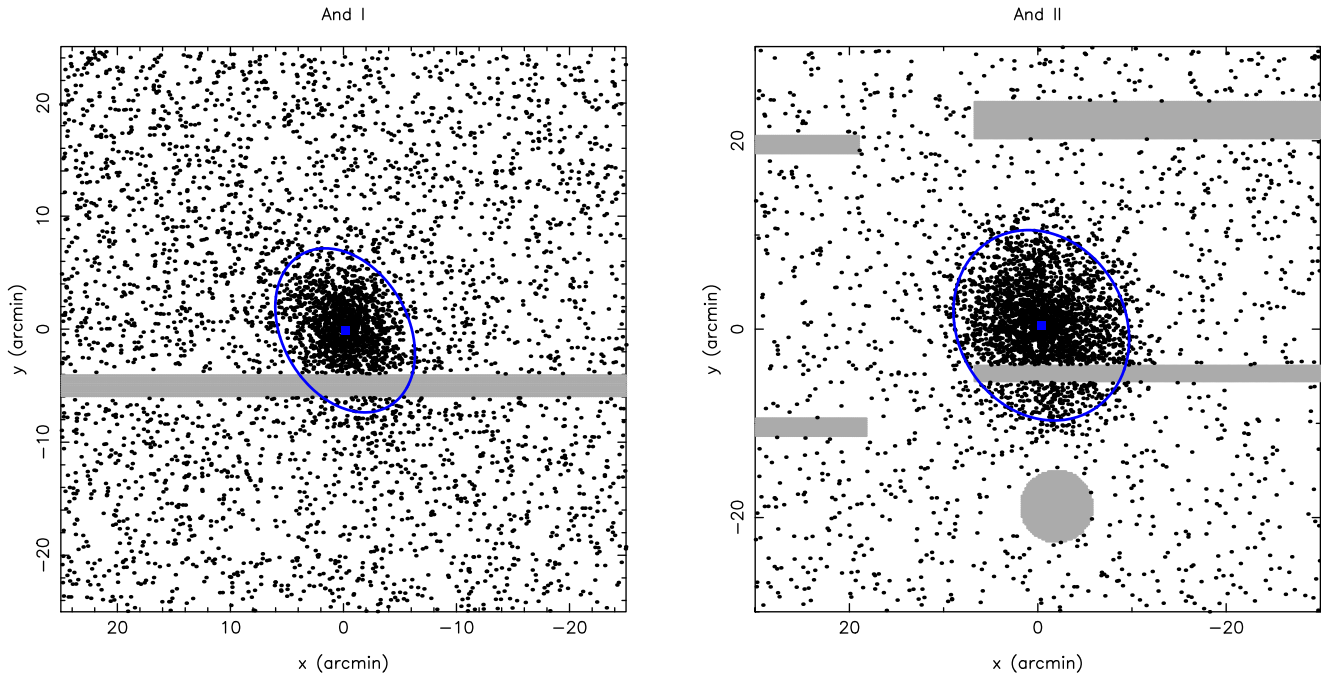
Figure 28. Distribution of CMD-selected stars in the region $\mathcal{A}$ around And I and And II. Regions in gray were masked out because of chip gaps, bright stars, or bad data. The represented (x,y) coordinates correspond to offsets from the chosen literature values of the centroid to the dwarf galaxies, as defined in Section 3.1. As such the favored centroids inferred from the current analysis and represented by the blue squares can be offset from (0, 0). The ellipses represent $2r_h$, as defined by the favored models.
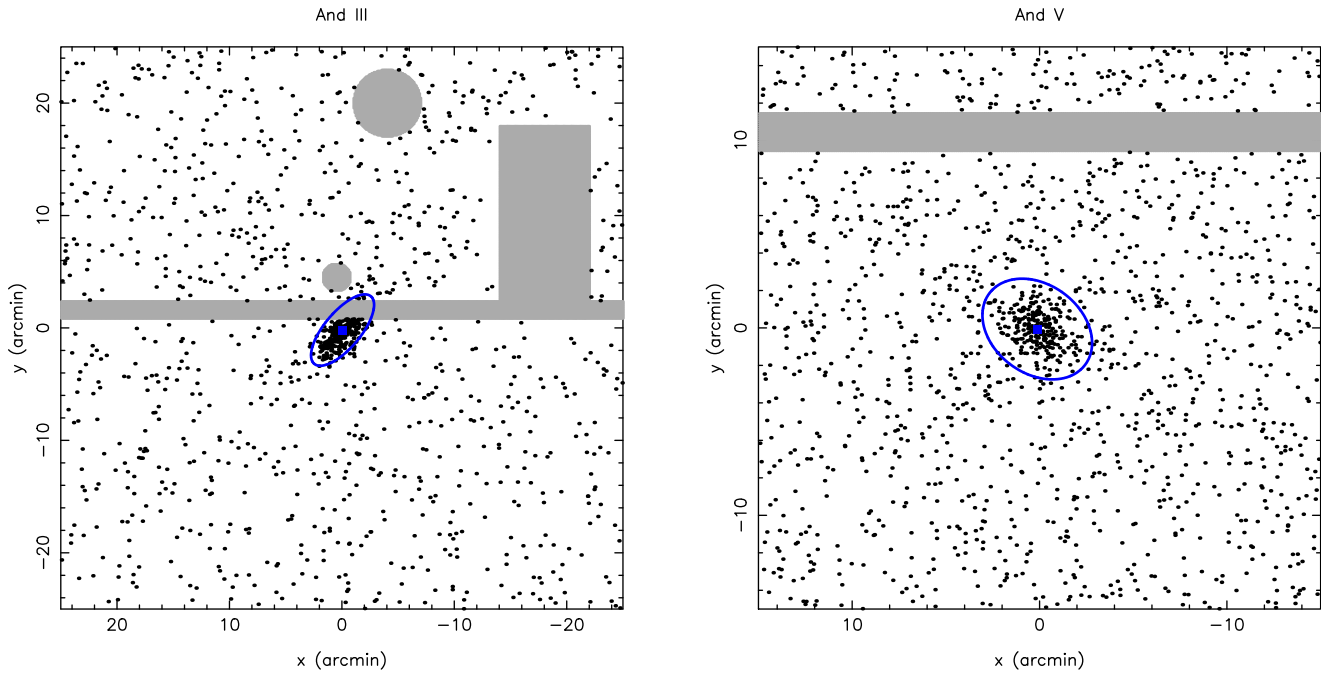
Figure 29. Same as Figure 28, but for And III and And V.

4.16. And XX

And XX is the last of the three dwarf galaxies discovered by McConnachie et al. (2008), who found it to be extremely small and faint ($r_h = 0.5 \pm 0\rlap{.}'1$, $\epsilon = 0.30 \pm 0.15$, $m_{V,0} = 18.2 \pm 0.8$). We concur with this assessment, as can be seen in Figure 20 ($r_h = 0.4^{+0.2}_{-0.1}{}'$, $\epsilon = 0.11^{+0.41}_{-0.11}$, $m_{V,0} = 18.0 \pm 0.4$). CMD "shot noise" is significant for this faint galaxy, but our technique that

relies on sampling artificial CMDs provides better constraints on $m_{V,0}$ than what was previously achieved by summing up the flux of the few observed stars.

4.17. And XXI

And XXI was found in PAndAS, and its first analysis was presented in Martin et al. (2009, $r_h = 3.5 \pm 0\rlap{.}'3$,
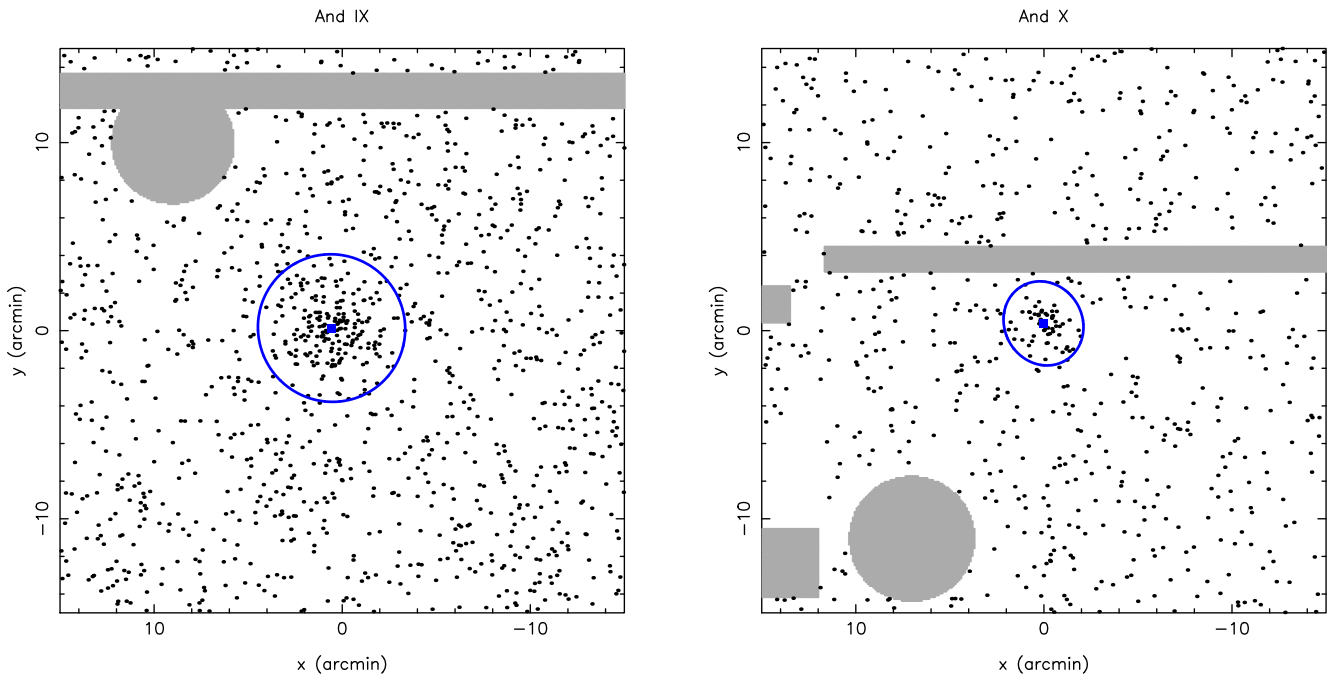
Figure 30. Same as Figure 28, but for And IX and And X.
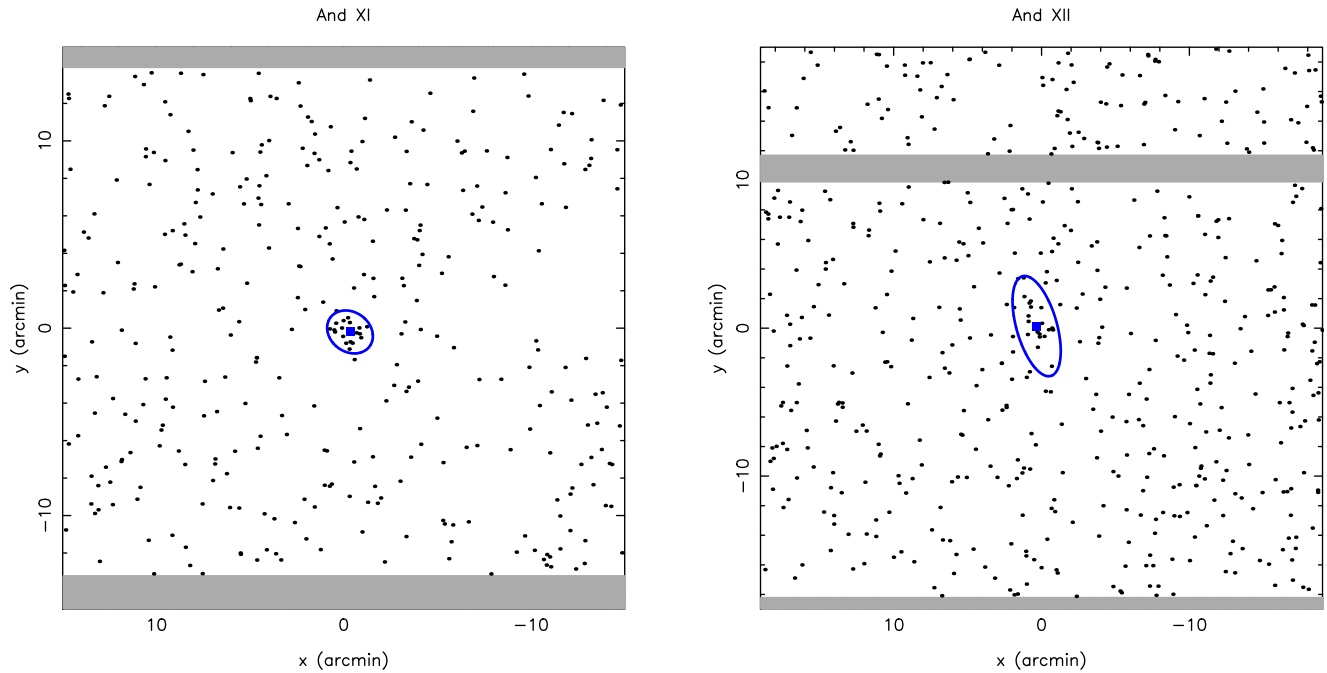

Figure 31. Same as Figure 28, but for And XI and And XII.

$\epsilon = 0.20 \pm 0.07$, $m_{V,0} = 14.8 \pm 0.6$). Our updated analysis yields results that are consistent with the literature values (Figure 21; $r_h = 4.1^{+0.8}_{-0.4}{}'$, $\epsilon = 0.36^{+0.10}_{-0.13}$, $m_{V,0} = 15.5 \pm 0.3$). The new magnitude measurement seems more consistent than the previous one if we are to compare the CMD of And XXI with that of other dwarf galaxies of similar apparent magnitude in Figure 2 (e.g., And V, And XXIII).

It should be noted that part of the central region of And XXI is masked out by a chip gap, which is naturally taken into account in the analysis.

4.18. And XXII

The discovery of And XXII is also presented in Martin et al. (2009, $r_h = 0.9 \pm 0.1{}'$, $\epsilon = 0.56 \pm 0.11$, $m_{V,0} = 18.0 \pm 0.8$), based on PAndAS data. The new analysis yields results in perfect agreement with this previous analysis of the same data (Figure 22; $r_h = 0.9^{+0.3}_{-0.2}{}'$, $\epsilon = 0.61^{+0.10}_{-0.14}$, $m_{V,0} = 18.0 \pm 0.4$), but with a better constrained magnitude measurement, despite a significant amount of CMD "shot noise." The new measurements also supersede the structural analysis of Chapman et al. (2013) based on the same data.
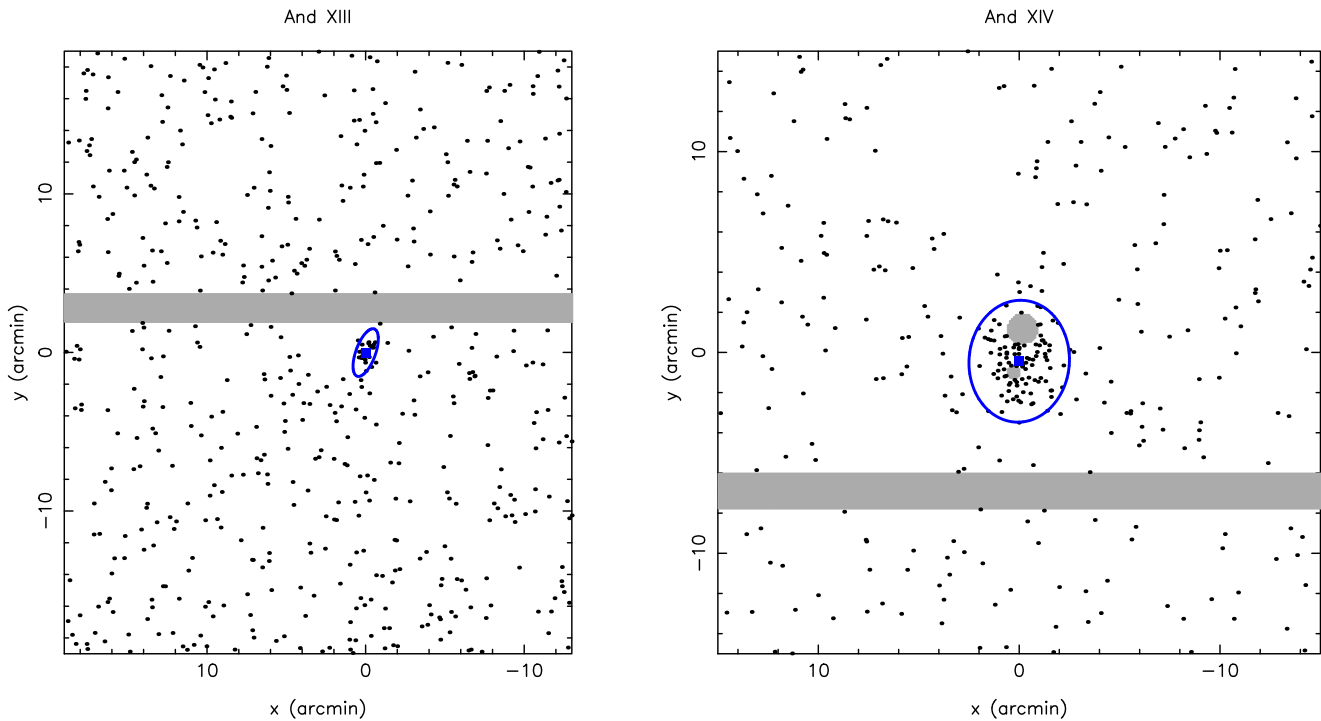
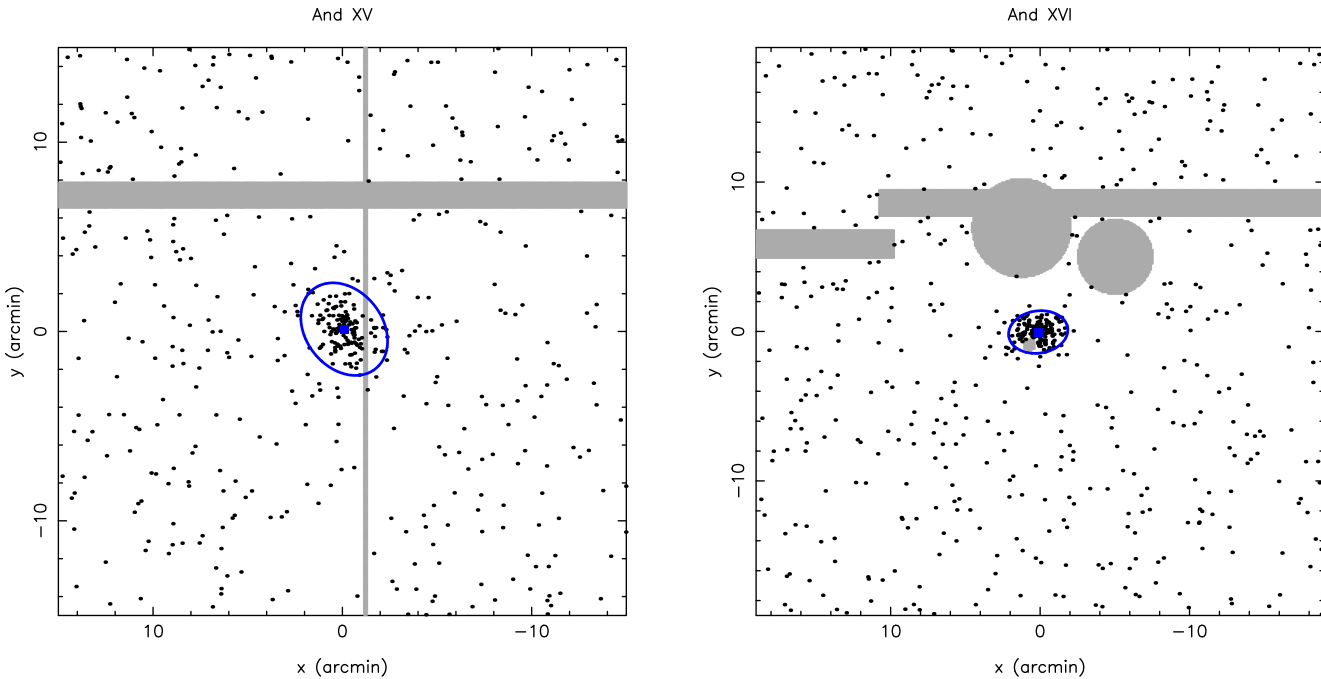**Figure 32.** Same as Figure 28, but for And XIII and And XIV.

Figure 33. Same as Figure 28, but for And XV and And XVI.

4.19. And XXIII

The discovery of And XXIII from PAndAS data is presented in Richardson et al. (2011, $r_h = 4.6 \pm 0'.2$, $\epsilon = 0.40 \pm 0.05$, $m_{V,0} = 14.2 \pm 0.5$), and our results (Figure 23; $r_h = 5.4 \pm 0'.4$, $\epsilon = 0.41^{+0.05}_{-0.06}$, $m_{V,0} = 14.6 \pm 0.2$) are in good agreement with this initial analysis, even though we now find the size to be slightly larger than originally estimated. And XXIII is among the most luminous M31 companions with an absolute magnitude of

$M_V = -9.8 \pm 0.1$, brighter even than And III and And V, but owes its late discovery to its large size and, therefore, its low surface brightness ($\mu_0 = 27.5 \pm 0.1$ mag arcsec^{-2}).

4.20. And XXIV

Like And XXIII, And XXIV was discovered in PAndAS by Richardson et al. (2011). The agreement is good between the initial estimate of this dwarf galaxy's parameters
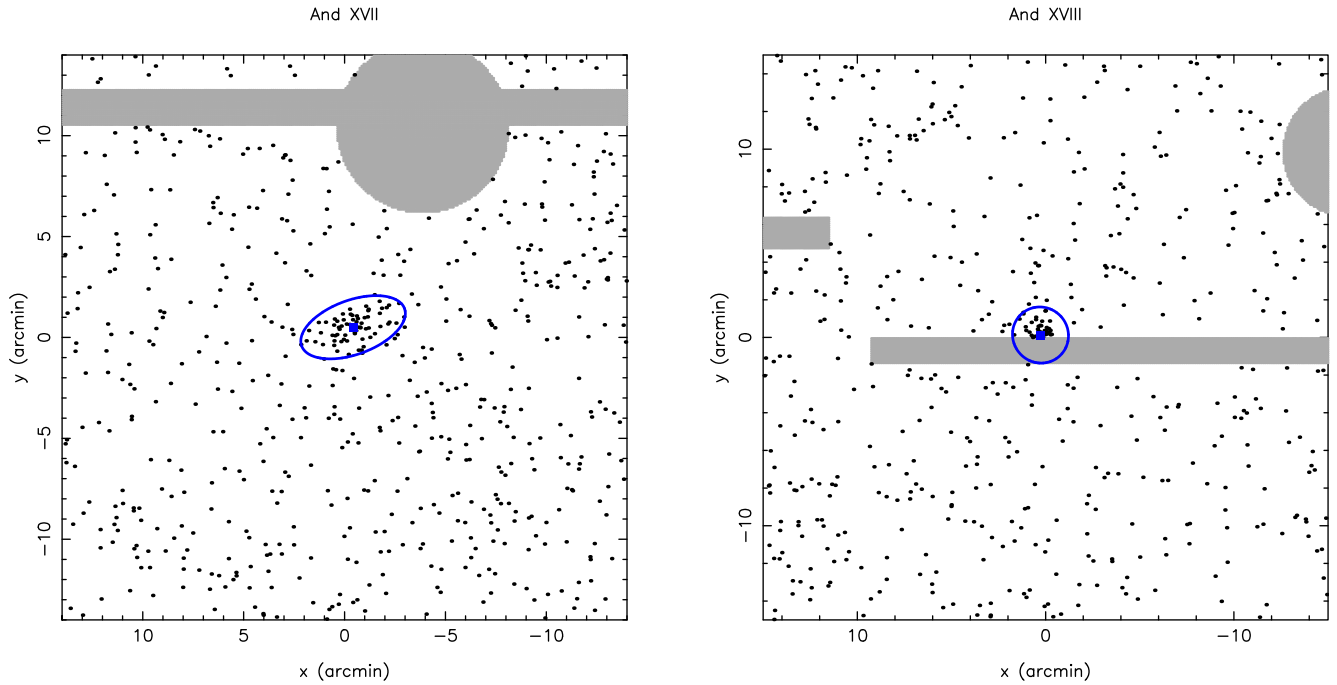
22

And XVII   And XVIII

Figure 34. Same as Figure 28, but for And XVII and And XVIII.
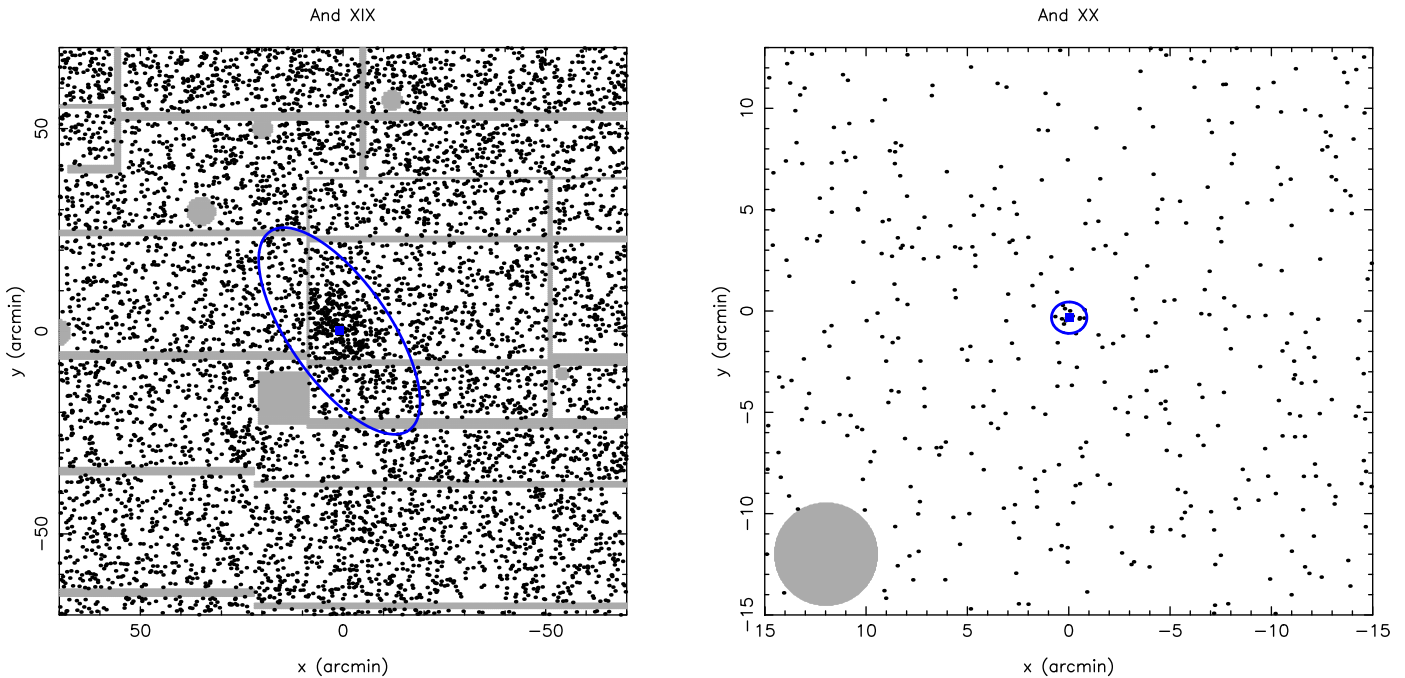
And XIX   And XX

Figure 35. Same as Figure 28, but for And XIX and And XX.

($r_h = 2.1 \pm 0\farcm1$, $\epsilon = 0.25 \pm 0.05$, $m_{V,0} = 16.3 \pm 0.5$) and our results (Figure 24; $r_h = 2.6^{+1.0}_{-0.5}{}'$, $\epsilon = 0.10^{+0.31}_{-0.10}$, $m_{V,0} = 16.3 \pm 0.3$). It should be noted that we had to mask a fairly large region a few arcminutes east of And XXIV because of bad-quality data at the edge of a PAndAS field (Figure 37).

fairly bright dwarf galaxy, as confirmed by our analysis (Figure 25; $r_h = 2.7^{+0.4}_{-0.2}{}'$, $\epsilon = 0.03^{+0.16}_{-0.03}$, $m_{V,0} = 15.3^{+0.3}_{-0.2}$). We find the system to be rounder than previously estimated, even though the two measurements are compatible. Part of the large uncertainties are the consequence of a large chip gap slicing through And XXV (Figure 38).

4.21. And XXV

And XXV was also found in PAndAS (Richardson et al. 2011, $r_h = 3.0 \pm 0\farcm3$, $\epsilon = 0.25 \pm 0.05$, $m_{V,0} = 14.8 \pm 0.5$). It is a

4.22. And XXVI

And XXVI was discovered in PAndAS (Richardson et al. 2011, $r_h = 1.0 \pm 0\farcm1$, $\epsilon = 0.25 \pm 0.05$, $m_{V,0} = 17.3 \pm 0.5$).
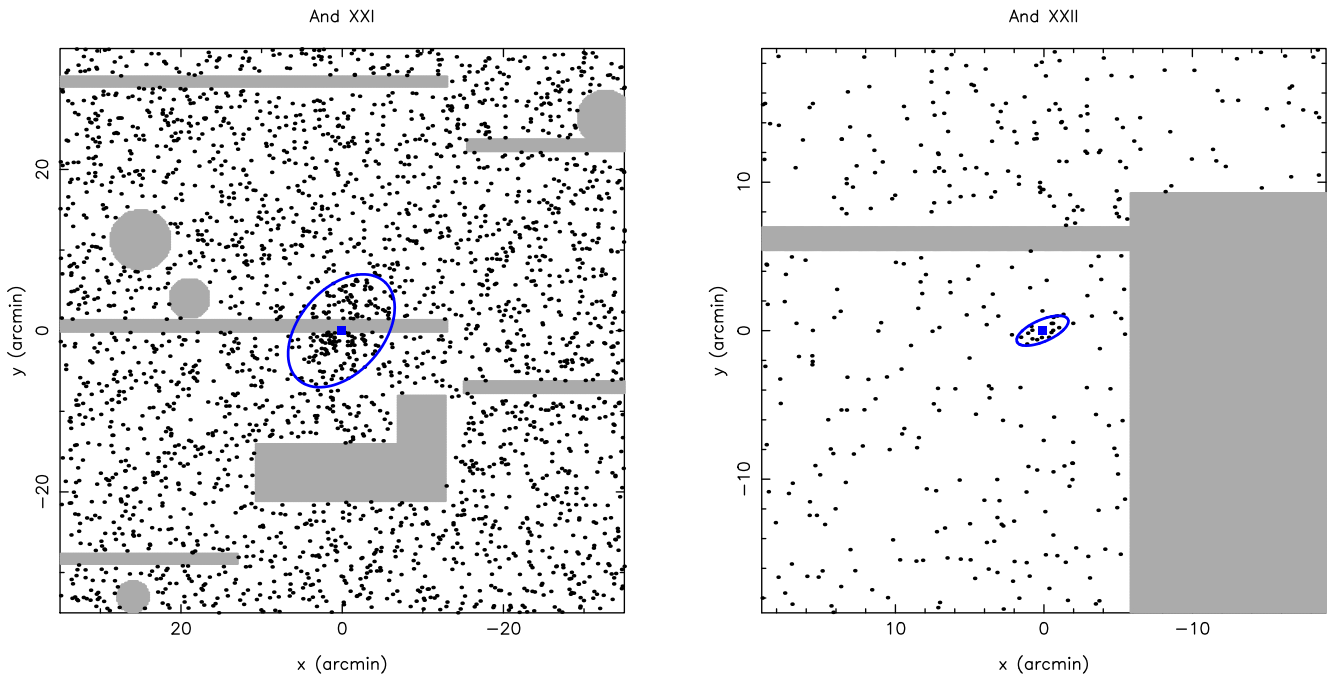
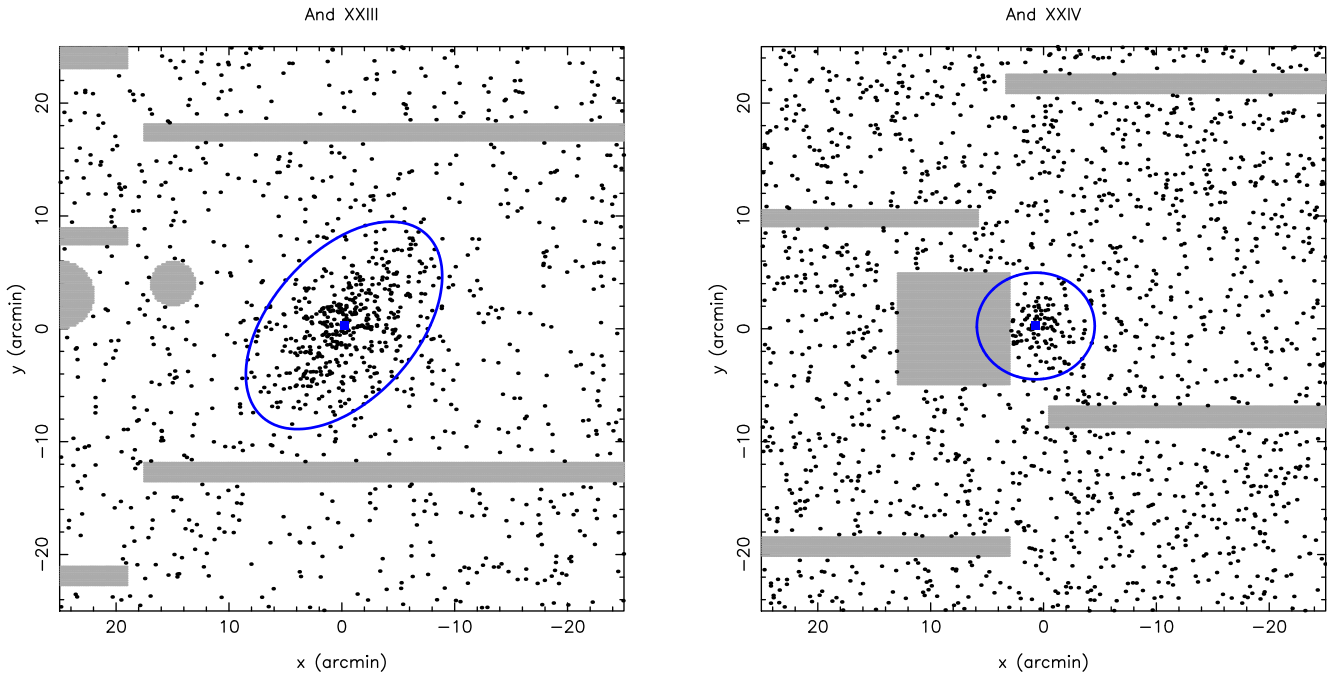**Figure 36.** Same as Figure 28, but for And XXI and And XXII.

Figure 37. Same as Figure 28, but for And XXIII and And XXIV.

The new analysis (Figure 26; $r_h = 1.0^{+0.6}_{-0.5}{}'$, $\epsilon = 0.35^{+0.33}_{-0.35}$, $m_{V,0} = 18.5^{+0.7}_{-0.5}$) hints that this could be the faintest dwarf galaxy known around M31, although our results are rendered noisy by And XXVI being located on one of the shallowest PAndAS fields and only a few arcminutes away from significant chip gaps (Figure 38). As a consequence, it was necessary to enforce an additional size prior ($r_{max} = 3'$) and centroid priors such that x_0 and y_0 do not deviate from the literature values by

more than $1'$. Once these are in place, the analysis converges on parameters that are representative of the dwarf galaxy.

4.23. Cas II/And XXX

Although Cas II/And XXX was mentioned in the PAndAS dwarf galaxy distance and spectroscopic study papers (Conn et al. 2012a; Collins et al. 2013), this is the first detailed analysis of its structure and luminosity (Figures 27 and 39).
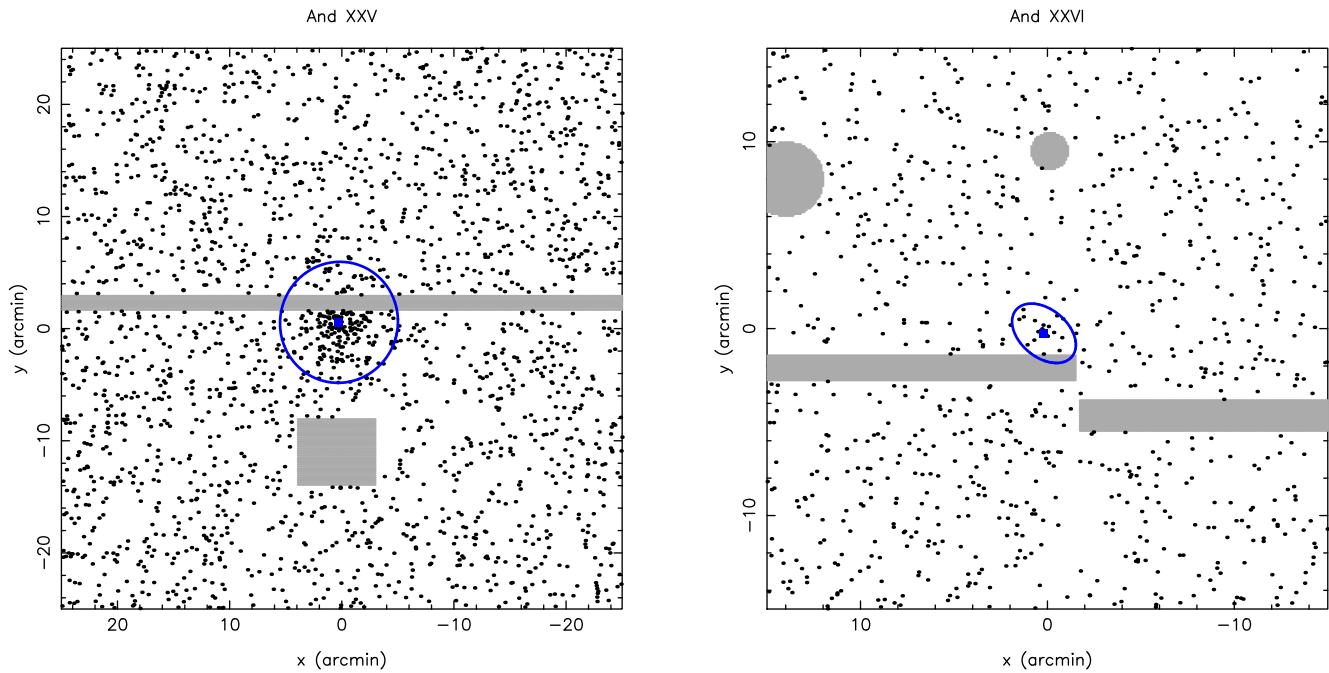
And XXV

And XXVI

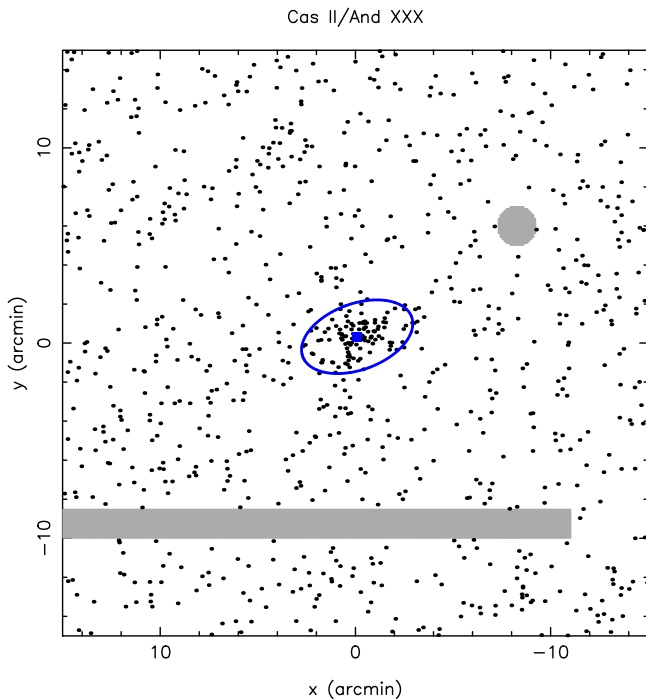**Figure 38.** Same as Figure 28, but for And XXV and And XXVI.

Cas II/And XXX

Figure 39. Same as Figure 28, but for Cas II/And XXX.

Located very close to NGC 147 and NGC 185, Cas II also shares distances (Conn et al. 2012b) and systemic velocities (Collins et al. 2013) that are close to those of these two large elliptical galaxies. It is therefore likely that the three galaxies are part of the same group[25] (Arias et al. 2016).

---

[25] Note, however, that Cas III/And XXXII (Martin et al. 2013c), located just outside the PAndAS footprint, north of NGC 147 and NGC 185, has a velocity that makes it incompatible with being part of this group of galaxies (Martin et al. 2014).

Cas II is reasonably faint ($m_{V,0} = 16.0^{+0.3}_{-0.2}$, $M_{V,0} = -8.0^{+0.4}_{-0.3}$) and has a typical size for galaxies of this luminosity ($r_h = 1.5 \pm 0'.2$ or 270 ± 50 pc). It is also quite elliptical ($\epsilon = 0.43^{+0.10}_{-0.12}$), although its major axis points neither toward NGC 147 nor toward NGC 185.

4.24. The Case of And XXVII

Despite there being a visual small overdensity of stars at the location of And XXVII reported by Richardson et al. (2011), it is impossible to get the algorithm to converge on a set of sensible parameters for this overdensity. The fit is entirely driven by the large stellar structure present in this region of the M31 stellar halo and favors an extremely large half-light radius ($r_h \sim 30'$) with only a few hundred stars ($N^* \sim 350$). Such a large half-light radius of ~ 6 kpc at the distance of M31 is implausible for a dwarf galaxy since, for the projected distance of And XXVII from M31 (~ 55 kpc), this is close to the tidal radius of a stellar system with $10^9\,M_\odot$. Even if And XXVII is located farther from M31, the stellar body of such a large system would likely still be significantly affected by tides. The structural parameters we infer more likely track the large stellar stream visible on the PAndAS stellar maps (e.g., Richardson et al. 2011). Already, the spectroscopic study of these stars by Collins et al. (2013) proved at odds with the expected properties of a dwarf galaxy as it revealed a large velocity dispersion of ~ 15 km s^{-1} and structure in the velocity distribution. The combination of peculiar kinematics and structural parameters lead us to conclude that And XXVII should not be classified as a dwarf galaxy and that we are likely observing a system that is in the final throes of its tidal disruption. A dedicated kinematic study shall hopefully shed more light on this system (J. Preston et al. 2016, in preparation).

5. CONCLUSIONS

We have presented a homogeneous study of the structure and luminosity of 23 M31 dwarf spheroidal galaxies from the contiguous photometric survey PAndAS. The structural parameter analysis presented here builds on the work of M08 and explicitly constructs the likelihood function from the positions of individual stars, using an exponential radial profile that allows for flattening and a constant level of contamination. One of the outputs of the model is the number of member stars in a chosen CMD selection box, which we tie to the apparent magnitude of a dwarf galaxy through the sampling of an artificial, representative CMD. This step naturally accounts for CMD "shot noise," which becomes significant for faint dwarf galaxies whose RGB is poorly sampled. The 23 dwarf spheroidal galaxies in PAndAS range in absolute magnitude from the luminous And II ($M_V = -11.6 \pm 0.2$), discovered more than 40 yr ago, to the very dim And XXVI ($M_V = -5.8^{+0.9}_{-1.0}$) discovered in PAndAS. Finally, we use the derived parameters to calculate the central surface brightnesses of the dwarf galaxies; these range from ~ 25 to ~ 29 mag arcsec^{-2}.

The main deviations from the literature values are as follows:

1. The luminosities of And XV and And XVI, which were significantly overestimated in our previous analysis. We now find that their total magnitudes are $M_V = -8.0^{+0.3}_{-0.4}$ and -7.3 ± 0.3, respectively.
2. The size of And XIX, which was significantly underestimated in our previous analysis and now yields $r_h = 3065^{+935}_{-1065}$ pc. This implies that And XIX is significantly affected by tides and/or that it is a local counterpart to the "extremely diffuse" galaxies recently found in the Coma Cluster (van Dokkum et al. 2015).
3. And XXVI is found to be significantly fainter than in its discovery paper with $m_V = 18.5^{+0.7}_{-0.5}$ and $M_V = -5.8^{+0.9}_{-1.0}$.
4. The impossibility to fit a sensible model to the stellar distribution around And XXVII, leading us to conclude, in conjunction with its peculiar kinematics, that it is not a dwarf galaxy but likely an unbound stellar structure in the M31 halo.

The Bayesian framework we place ourselves in (sampling the prior PDFs on the distance and other relevant parameters) allows us to straightforwardly track the impact of uncertainties on the derived parameters. We further provide samplings from the Monte Carlo Markov Chains generated by our analysis in Appendix B; these correspond to much more truthful representations of the analysis than the parameters listed in Tables 1 and 2. Anyone who wishes to properly account for degeneracies between the parameters as well as for the peculiarity of the PDFs should strive to use these chains in their own analysis.

Combined with the Conn et al. (2012a) inference of distance to these systems from the same data, the properties listed in Table 1 and their PDFs provide a characterization of a populated dwarf galaxy satellite system that should be free of most systematics that usually plague analyses based on data gathered in the literature, originating from different telescopes and instruments, and analyzed with different techniques.[26] The benefits of this data set have started to be exploited in studies of

the global properties of the M31 dwarf galaxies, such as a comparison of the properties of dwarf galaxies in and out of the vast and thin rotating disk of M31 satellites (Ibata et al. 2013), as recently presented by Collins et al. (2015); a recent study of the alignment of M31 satellites with their host (Barber et al. 2015); or a study of the intrinsic shape of the M31 satellite dwarf galaxies (Salomon et al. 2015).

Once we have determined the dwarf galaxy search completeness functions in the next paper in this series, we will endeavor to reliably characterize the global properties of a large fraction of the M31 dwarf galaxy system.

APPENDIX A
STELLAR DISTRIBUTIONS

Figures 28–39 show the stellar distribution $\mathcal{D}_n$ that was used for each dwarf galaxy. Each map corresponds to the region $\mathcal{A}$ of a given system, with masked-out regions indicated in gray. The favored model, determined from the modes of the structural parameters' distributions, is shown as the blue ellipses that represent the $2r_h$ region. The blue square locates the favored centroid (x_0, y_0).

APPENDIX B
CHAINS

A sampling of the chains generated by the algorithm is available online in electronic tabular form for the 23 dwarf spheroidal galaxies discussed in the paper. Each table contains 500 randomly selected drawings from each chain. Table 3 provides an excerpt of the And I chain for illustration. For each line, corresponding to a single drawing, columns (1) and (2) list the right ascension and declination of the centroid, column (3) gives the ellipticity ϵ, and column (4) gives the position angle θ. Columns (5) and (6) give the half-light radius r_h in arcminutes and then in parsecs, as determined using a distance modulus value (listed further) randomly drawn from the relevant chain provided by Conn et al. (2012a). Column (7) lists the apparent magnitude $m_{V,0}$, while column (8) lists absolute magnitude $M_{V,0}$, once again determined using the same distance modulus value as above. Column (9) gives the logarithm of the luminosity of the dwarf galaxy, while column (10) lists the central surface brightness in units of magnitudes per arcsec^2. Finally, column (11) gives the distance modulus value that was used to determine the relevant parameters. Note that the distance modulus values are drawn from the Conn et al. (2012a) chains and were not derived in this paper.

---

[26] Although derived from another survey, it should also be noted that the structural parameters derived for Cas III/And XXXI, Lac I/And XXXII, and Per I/And XXXIII, three M31 dwarf galaxies discovered in Pan-STARRS1 data (Martin et al. 2013b, 2013c), were derived using the algorithm presented here.

Table 3
Excerpt from the And I Chain Online Table

α (deg) (1)	δ (deg) (2)	ϵ (3)	θ (deg) (4)	r_h (arcmin) (5)	r_h (pc) (6)	$m_{V,0}$ (7)	$M_{V,0}$ (8)	$\log_{10}(L_V/L_\odot)$ (9)	μ_0 (mag arcsec^{-2}) (10)	Distance Modulus (11)
11.414190	+38.037327	0.29	30.2	3.87	800	12.9	−11.3	6.42	25.26	24.26
11.415506	+38.036674	0.31	28.6	3.97	848	13.1	−11.3	6.40	25.41	24.33
11.412939	+38.037632	0.25	23.4	3.71	796	13.2	−11.2	6.37	25.46	24.34
11.415737	+38.036972	0.25	33.7	3.75	801	13.4	−10.9	6.27	25.72	24.33
11.413170	+38.035038	0.30	31.7	4.06	843	13.0	−11.3	6.41	25.40	24.27
11.413185	+38.034157	0.31	26.2	4.02	847	13.2	−11.1	6.32	25.61	24.30
11.415273	+38.037071	0.32	33.6	4.07	877	13.0	−11.3	6.43	25.40	24.35
11.416187	+38.035320	0.25	28.4	3.78	858	13.1	−11.3	6.42	25.47	24.46
11.414933	+38.037369	0.25	30.4	3.72	814	13.3	−11.1	6.34	25.56	24.38
11.414639	+38.036373	0.24	26.1	3.87	865	13.3	−11.1	6.34	25.73	24.43

REFERENCES

Amorisco, N. C., Evans, N. W., & van de Ven, G. 2014, Natur, 507, 335
Arias, V., Guglielmo, M., Fernando, N., et al. 2016, MNRAS, 456, 1654
Armandroff, T. E., Davies, J. E., & Jacoby, G. H. 1998, AJ, 116, 2287
Barber, C., Starkenburg, E., Navarro, J. F., & McConnachie, A. W. 2015, MNRAS, 447, 1112
Bate, N. F., Conn, A. R., McMonigal, B., et al. 2014, MNRAS, 437, 3362
Bell, E. F., Slater, C. T., & Martin, N. F. 2011, ApJL, 742, L15
Belokurov, V. 2013, NewAR, 57, 100
Brasseur, C. M., Martin, N. F., Macciò, A. V., Rix, H.-W., & Kang, X. 2011a, ApJ, 743, 179
Brasseur, C. M., Martin, N. F., Rix, H.-W., et al. 2011b, ApJ, 729, 23
Bressan, A., Marigo, P., Girardi, L., et al. 2012, MNRAS, 427, 127
Chabrier, G. 2001, ApJ, 554, 1274
Chapman, S. C., Widrow, L., Collins, M. L. M., et al. 2013, MNRAS, 430, 37
Collins, M. L. M., Chapman, S. C., Irwin, M. J., et al. 2010, MNRAS, 407, 2411
Collins, M. L. M., Chapman, S. C., Rich, R. M., et al. 2011, MNRAS, 417, 1170
Collins, M. L. M., Chapman, S. C., Rich, R. M., et al. 2013, ApJ, 768, 172
Collins, M. L. M., Martin, N. F., Rich, R. M., et al. 2015, ApJL, 799, L13
Conn, A. R., Ibata, R. A., Lewis, G. F., et al. 2012a, ApJ, 758, 11
Conn, A. R., Lewis, G. F., Ibata, R. A., et al. 2011, ApJ, 740, 69
Conn, B. C., Noël, N. E. D., Rix, H.-W., et al. 2012b, ApJ, 754, 101
Crnojević, D., Ferguson, A. M. N., Irwin, M. J., et al. 2014, MNRAS, 445, 3862
de Jong, J. T. A., Rix, H.-W., Martin, N. F., et al. 2008, AJ, 135, 1361
Faber, S. M., & Lin, D. N. C. 1983, ApJL, 266, L17
Fardal, M. A., Guhathakurta, P., Babul, A., & McConnachie, A. W. 2007, MNRAS, 380, 15
Ferguson, A. M. N., Irwin, M. J., Ibata, R. A., Lewis, G. F., & Tanvir, N. R. 2002, AJ, 124, 1452
Gilmore, G., Wilkinson, M. I., Wyse, R. F. G., et al. 2007, ApJ, 663, 948
Grebel, E. K., & Gallagher, J. S., III 2004, ApJL, 610, L89
Ho, N., Geha, M., Tollerud, E. J., et al. 2015, ApJ, 798, 77
Ibata, R., Irwin, M., Lewis, G., Ferguson, A. M. N., & Tanvir, N. 2001, Natur, 412, 49
Ibata, R., Martin, N. F., Irwin, M., et al. 2007, ApJ, 671, 1591
Ibata, R. A., Lewis, G. F., Conn, A. R., et al. 2013, Natur, 493, 62
Ibata, R. A., Lewis, G. F., McConnachie, A. W., et al. 2014, ApJ, 780, 128
Irwin, M., & Lewis, J. 2001, NewAR, 45, 105
Irwin, M. J., Ferguson, A. M. N., Huxor, A. P., et al. 2008, ApJL, 676, L17
Kalirai, J. S., Beaton, R. L., Geha, M. C., et al. 2010, ApJ, 711, 671

Majewski, S. R., Beaton, R. L., Patterson, R. J., et al. 2007, ApJL, 670, L9
Majewski, S. R., Skrutskie, M. F., Weinberg, M. D., & Ostheimer, J. C. 2003, ApJ, 599, 1082
Martin, N. F., Chambers, K. C., Collins, M. L. M., et al. 2014, ApJL, 793, L14
Martin, N. F., de Jong, J. T. A., & Rix, H.-W. 2008, ApJ, 684, 1075
Martin, N. F., Ibata, R. A., Chapman, S. C., Irwin, M., & Lewis, G. F. 2007, MNRAS, 380, 281
Martin, N. F., Ibata, R. A., Irwin, M. J., et al. 2006, MNRAS, 371, 1983
Martin, N. F., Ibata, R. A., McConnachie, A. W., et al. 2013a, ApJ, 776, 80
Martin, N. F., McConnachie, A. W., Irwin, M., et al. 2009, ApJ, 705, 758
Martin, N. F., Schlafly, E. F., Slater, C. T., et al. 2013b, ApJL, 779, L10
Martin, N. F., Slater, C. T., Schlafly, E. F., et al. 2013c, ApJ, 772, 15
Mateo, M. L. 1998, ARA&A, 36, 435
McConnachie, A. W. 2012, AJ, 144, 4
McConnachie, A. W., Arimoto, N., & Irwin, M. 2007, MNRAS, 379, 379
McConnachie, A. W., Huxor, A., Martin, N. F., et al. 2008, ApJ, 688, 1009
McConnachie, A. W., & Irwin, M. J. 2006, MNRAS, 365, 1263
McConnachie, A. W., Irwin, M. J., Ibata, R. A., et al. 2009, Natur, 461, 66
Muñoz, R. R., Padmanabhan, N., & Geha, M. 2012, ApJ, 745, 127
Pawlowski, M. S., & McGaugh, S. S. 2014, ApJL, 789, L24
Read, J. I., & Gilmore, G. 2005, MNRAS, 356, 107
Richardson, J. C., Irwin, M. J., McConnachie, A. W., et al. 2011, ApJ, 732, 76
Sales, L. V., Navarro, J. F., Abadi, M. G., & Steinmetz, M. 2007, MNRAS, 379, 1464
Salomon, J.-B., Ibata, R. A., Martin, N. F., & Famaey, B. 2015, MNRAS, 450, 1409
Schlafly, E. F., & Finkbeiner, D. P. 2011, ApJ, 737, 103
Schlegel, D. J., Finkbeiner, D. P., & Davis, M. 1998, ApJ, 500, 525
Simon, J. D., & Geha, M. 2007, ApJ, 670, 313
Skillman, E. D., Monelli, M., Weisz, D. R., et al. 2016, ApJ, submitted (arXiv:1606.01207)
Slater, C. T., Bell, E. F., & Martin, N. F. 2011, ApJL, 742, L14
Tolstoy, E., Hill, V., & Tosi, M. 2009, ARA&A, 47, 371
Tolstoy, E., Irwin, M. J., Helmi, A., et al. 2004, ApJL, 617, L119
van den Bergh, S. 1972, ApJL, 171, L31
van Dokkum, P. G., Abraham, R., Merritt, A., et al. 2015, ApJL, 798, L45
Weisz, D. R., Dolphin, A. E., Skillman, E. D., et al. 2014a, ApJ, 789, 147
Weisz, D. R., Dolphin, A. E., Skillman, E. D., et al. 2014b, ApJ, 789, 148
Weisz, D. R., Skillman, E. D., Hidalgo, S. L., et al. 2014c, ApJ, 789, 24
Willman, B., & Strader, J. 2012, AJ, 144, 76
Zucker, D. B., Kniazev, A. Y., Bell, E. F., et al. 2004, ApJL, 612, L121
Zucker, D. B., Kniazev, A. Y., Martínez-Delgado, D., et al. 2007, ApJL, 659, L21